Short heat shock factor A2 confers heat sensitivity in *Arabidopsis*: Insights into heat resistance and growth balance

Wanxia Chen[1], Jiaqi Zhao[1], Zhanxia Tao[1], Shan Zhang[1], Xiujuan Bei[1], Wen Lu[1], and Xiaoting Qi[1]*

[1]College of Life Sciences, Capital Normal University, Beijing 100048, China.

*Corresponding author (qixiaoting@cnu.edu.cn)

ORCID: 0000-0001-7172-2391

Short title: A noncanonical heat shock response

Total words: 11220

Figures: 11

Supplementary Figures: 9

Supplementary Tables: 2

Abstract

Cells prevent heat damage through a highly conserved canonical heat stress response (HSR) in which heat shock factors (HSFs) bind heat shock elements (HSEs) to activate heat shock proteins (HSPs). Plants generate short HSFs that originate from HSF splicing variants, but little is known about S-HSFs. Although an enhanced canonical HSR confers thermotolerance, its hyperactivation inhibits plant growth. How this process is prevented to ensure proper plant growth has not been determined. Here, we report that *Arabidopsis* S-HsfA2, S-HsfA4c, and S-HsfB1 confer extreme heat (45°C) sensitivity and represent new kinds of HSF with a unique truncated DNA-binding domain (tDBD) that binds a new heat-regulated element (HRE). The HRE conferred a minimal promoter response to heat and exhibited heat stress sensing and transmission patterns. We used S-HsfA2 to investigate whether and how S-HSFs prevent hyperactivation of the canonical HSR. *HSP17.6B*, a direct target gene of HsfA2, conferred thermotolerance, but its overexpression caused HSR hyperactivation. We revealed that S-HsfA2 alleviated this hyperactivation in two different ways. 1) S-HsfA2 negatively regulates *HSP17.6B via* the HRE-HRE-like element, thus constructing a noncanonical HSR (S-HsfA2-HRE-*HSP17.6B*) to antagonistically repress HsfA2-activated *HSP17.6B* expression. 2) S-HsfA2 binds to the DBD of HsfA2 to prevent HsfA2 from binding to HSEs, eventually attenuating HsfA2-activated *HSP17.6B* promoter activity. Overall, our findings underscore the biological importance of S-HSFs, namely, preventing plant heat tolerance hyperactivation to maintain proper growth.

Graphical Abstract

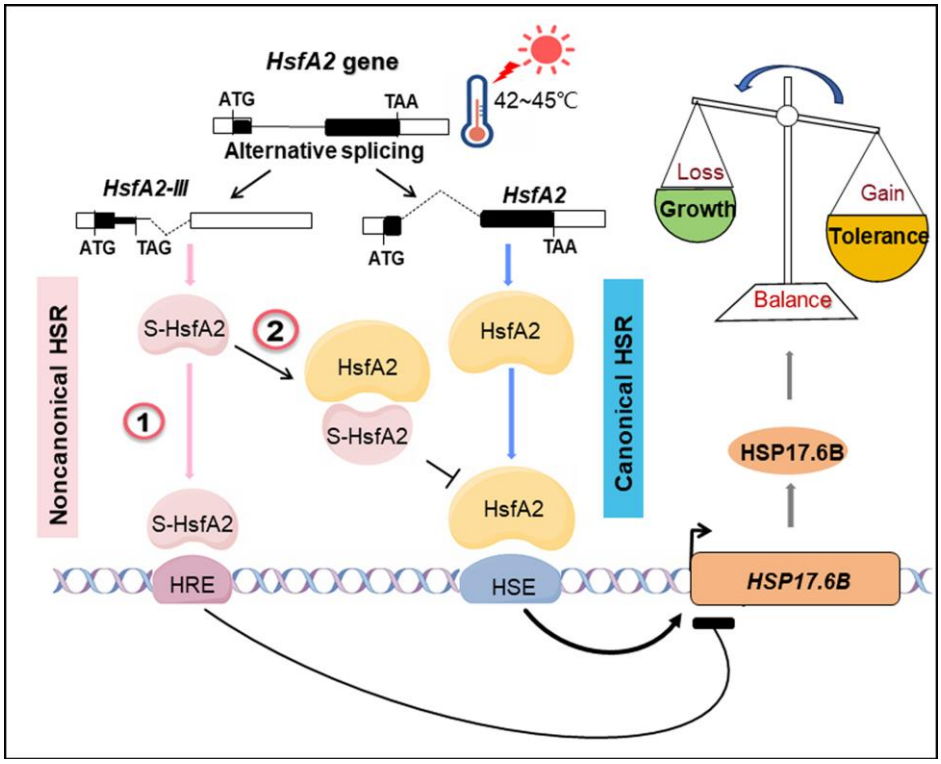

Introduction

Elevated temperatures, *i.e.*, heat shock or heat stress, have become a global problem threatening crop yields (Bita and Gerats, 2013). Cells prevent heat damage through the canonical heat stress response (HSR). In this canonical HSR, a heat shock factor (HSF) trimer binds a DNA *cis*-acting element called a heat shock element (HSE) to induce the production of heat shock proteins (HSPs). This canonical HSR is highly conserved among different organisms but is highly complex in plants (Morimoto, 1993). Accordingly, heat-tolerant plants are usually generated by overexpressing *HSFs* or *HSPs* (Fragkostefanakis et al., 2015). Several studies have revealed that enhanced canonical HSR is beneficial for plant heat tolerance but also results in growth inhibition under normal conditions. Zhu et al. (2009) reported that overexpression of *Boea hygrometrica Hsf1* in *Arabidopsis* and tobacco confers plant thermotolerance but also leads to seedling dwarfism under normal conditions. When *Arabidopsis HsfA2* and *HsfA3* are overexpressed, these *Arabidopsis* plants tolerate increased heat stress but exhibit seedling dwarfism under nonstress conditions (Ogawa et al., 2007; Yoshida et al., 2008). These findings reflect the active growth inhibition of canonical HSR hyperactivation under nonstress conditions, which is undesirable for plant productivity. However, much less is known about how plants prevent canonical HSR hyperactivation to ensure a balance between heat resistance and growth. Considering that HSRs are highly complex in plants, we reasoned that there should be new kinds of HSFs that inhibit canonical HSR hyperactivation in plants. However, these new kinds of HSFs and their underlying regulatory mechanisms have yet to be determined in plants.

A common way for introns to expand the diversity of host gene products is alternative splicing (AS). An increasing number of studies have shown that heat

stress-induced AS events in heat response genes, including HSFs, are very important regulatory mechanisms for the fitness of plants under heat stress (Ling et al., 2021). Thus, we focused on heat-induced AS events in HSFs as a starting point for revealing new kinds of HSFs and their functions and regulatory mechanisms in the plant response to heat stress.

HSFs share similar constructs across eukaryotes, in which the HSE DNA-binding domain (DBD) is the most conserved (Nover et al., 2001). The DBD is a “winged” helix-turn-helix protein that consists of three α-helices (H1, H2, H3) and four-stranded antiparallel β-sheets (β1, β2, β3, β4). H3 directly binds to the HSE, and its adjacent wing domain (β3-loop-β4) is needed for the formation of HSF-HSE trimers (Littlefield and Nelson, 1999; Ahn et al., 2001; Feng et al., 2021). Interestingly, for all HSFs, the position of an intron within the DBD is conserved (Nover et al., 2001), and the intron is inserted between H3 and the wing domain coding region. In plants, mostly under heat stress, this intron is fully or partially retained to generate splice variants, such as *Arabidopsis HsfA2-II* (Sugio et al., 2009), *Arabidopsis HsfA2-III* (Liu et al., 2013), rice (*Oryza sativa*) *OsHSFA2dII* (Cheng et al., 2015), lily (*Lilium* spp.) *LlHSFA3B-III* (Wu et al. 2019), wheat (*Triticum aestivum*) *TaHsfA2-7-AS* (Ma et al., 2023), and maize (*Zea mays*) *ZmHsf17-II* (Zhang et al., 2024). These variants contain in-frame stop codons within the retained intron that may translate into short HSF isoforms (S-HSFs).

Several S-HSFs have been proven to play regulatory roles in thermotolerance in plants. Previously, we reported that heat stress-induced S-HsfA2 was detected by immunoblotting and can regulate the expression of *HsfA2* by binding to HSEs within the *HsfA2* promoter (Liu et al., 2013). Wu et al. (2019) also reported that LlHSFA3B-III (S-LIHSFA3B) can be detected by immunoblotting and that overexpressing *S-HSFA3B* reduces tolerance to acute heat (45°C) in *Arabidopsis* plants. TaHsfA2-7 generates the splice variant TaHsfA2-7-AS (S-TaHsfA2-7), which confers tolerance to heat (45°C) in *Arabidopsis* (Ma et al., 2023).

S-LIHSFA3B interacts with lily HSFA3A to limit its transactivation function and temper the function of lily HSFA3A (Wu et al., 2019). S-ZmHsf17 can interact with the DBD of full-length ZmHsf17 to suppress the transactivation of ZmHsf17 (Zhang et al., 2024). These findings suggest that S-HSFs can regulate the activities of HSFs through S-HSF–HSF protein interactions. However, how S-HSFs, as transcription factors, regulate plant heat responses remains unclear. Unlike classical HSFs, S-HSFs contain a unique C-terminal truncated DBD (tDBD) and an extended motif or domain encoded by the retained intron sequences (Liu et al., 2013). Although S-HSFs lack nuclear localization signals, S-HSFs can also localize to the nucleus (Sugio et al., 2009; Liu et al., 2013; Cheng et al., 2015; Wu et al. 2019; Ma et al., 2023; Zhang et al., 2024). The tDBD lacks a wing domain and thereby might enable S-HSFs to recognize new heat-responsive DNA elements related to the HSE, while extended motifs or domains are variable in length and sequence and subsequently might contribute to regulatory roles, such as transcriptional regulation. Thus, S-HSFs could represent new kinds of plant HSFs. Considering that unique S-HSFs are expressed mostly under extreme heat stress, they could be associated with plant responses to heat stress. Therefore, uncovering the mechanism through which canonical HSR hyperactivation is regulated by S-HSFs will shed light on the balance between growth and thermotolerance.

In this study, we reported that S-HSFs (*i.e.*, S-HsfA2, S-HsfA4c, and S-HsfB1) are new kinds of HSFs that bind new heat-regulated elements (HREs) and negatively regulate *Arabidopsis* tolerance to extreme heat stress. Using S-HsfA2 as a representative S-HSF, we further investigated the molecular mechanisms by which S-HSFs prevent canonical HSR hyperactivation. The results showed that S-HsfA2 alleviates *HSP17.6B* overexpression-mediated HSR hyperactivation in two different ways: antagonistically repressing *HSP17.6B* overexpression through a noncanonical HSR (S-HsfA2-HRE-*HSP17.6B*) and acting as a negative binding regulator of HSFs to inhibit the binding of HsfA2 to the HSE of the HSP17.6B promoter. Our results reveal

new kinds of HSF originating from HSF splicing variants and provide deep mechanistic insights into proper growth control against thermotolerance hyperactivity in plants.

Results

S-HsfA2 confers extreme heat (45°C) sensitivity in *Arabidopsis*

S-HsfA2 contains a 42-aa N-terminal domain (N-ter), a 61-aa tDBD, and a 26-aa extended leucine (L)-rich domain (LRD) (Figure 1A). According to the predicted AlphaFold 3D structure of S-HsfA2, the LRD forms an α-helix structure. Given that S-HsfA2 is expressed under extreme heat (42°C) but not under moderate heat (37°C) (Liu et al., 2013), we determined its role in tolerance to extreme heat. Overexpression of Flag-tagged S-HsfA2 under the control of the cauliflower mosaic virus 35S RNA promoter (35S) (*35S:S-HsfA2-Flag*, S-HsfA2-OE) significantly reduced seedling survival at 45°C for 2 h compared to that of the wild-type (WT) control (Figure 1B).

Our previous study showed that LRD is responsible for the transcriptional repression of S-HsfA2 in yeast cells (Liu et al., 2013). We noted that a conserved transcriptional repression motif, LxLxLx (x=any amino acid) (Tiwari and Guilfoyle, 2004), exists in the LRD (Figure 1A). Mutations (L to alanine (A)) in the LxLxLx motif (S-HsfA2$^{L\text{-}A}$) converted S-HsfA2 from a transcriptional repressor to a transcriptional activator in yeast cells (Supplemental Figure S1), indicating that S-HsfA2 is an LxLxLx-type transcriptional repressor. As a result, overexpression of this dominant activator of S-HsfA2-Flag (S-HsfA2$^{L\text{-}A}$-OE) eliminated the extreme heat-sensitive phenotype (Figure 1B). When the plants were grown in soil, the S-HsfA2 genetic plants also exhibited the same extreme heat response phenotype (Figure 1B).

Next, we generated S-HsfA2-encoding mRNA (*HsfA2-III*)-knockdown transgenic lines (S-HsfA2-KD) through RNA interference (RNAi) (Figure 1C). In

S-HsfA2-KD, the abundance of *HsfA2-III* but not *HsfA2-II* or *HsfA2* mRNA decreased under heat stress. S-HsfA2-KD plants displayed a clear resistance phenotype to extreme heat in both medium and soil (Figure 1C). Overall, these genetic data strongly confirm that S-HsfA2 is sensitive to extreme heat in *Arabidopsis* and that the LxLxLx motif is needed for its biological functions.

The constitutive expression of S-HsfA2 inhibits *Arabidopsis* seedling growth

We also noted that overexpression of S-HsfA2 (S-HsfA2-OE) caused short root length (growth in medium) and seedling dwarfism (growth in soil) under normal conditions (Supplemental Figure S2). However, these growth defects were partially rescued in the S-HsfA2L-A-OE seedlings (Supplemental Figure S2), suggesting that the LxLxLx motif of S-HsfA2 is required for these biological functions. This finding reflected the negative impact of the constitutive expression of S-HsfA2 on *Arabidopsis* seedling growth.

Heat stress promotes the nuclear accumulation of S-HsfA2

A previous study showed that S-HsfA2 is localized in the nucleus of *Arabidopsis* mesophyll protoplasts (Liu et al., 2013). We further investigated the subcellular localization of S-HsfA2 in *Arabidopsis* using the *35S:S-HsfA2-GFP* transgene. We found that the GFP signals were distributed throughout the root cells under normal conditions but that the signals accumulated mainly in the nucleus after heat stress treatment (Supplemental Figure S3). This result is consistent with the finding that S-HsfA2 is a transcription factor involved in heat stress regulation.

S-HsfA2 binds a *cis*-acting element termed the heat-regulated element (HRE)

As S-HsfA2 is a transcription factor with a unique tDBD, we identified new *cis*-acting elements other than HSEs recognized by S-HsfA2 through chromatin immunoprecipitation (ChIP) in heat stress-treated *35S:S-HsfA2-GFP* transgenic *Arabidopsis* (Supplemental Figure S4A). High-throughput sequencing (seq) of DNA

precipitated with an anti-GFP antibody revealed a centrosymmetric 7-bp motif (5′-GAAGAAG-3′). This motif was most significantly enriched ($E=10^{-19}$) in the ChIP-Seq dataset (Supplemental Figure S4B). Because it was demonstrated to be a heat-regulated element, we hereafter named it an HRE.

HSEs are composed of at least three alternating nGAAn/nTTCn blocks (n denotes any nucleotide) (Amin et al., 1988). Accordingly, an HRE is considered a partially overlapping element of two inverted nGAAn blocks sharing a G base (5′-nGAA->G<-AAGn-3′), indicating that the HRE and HSE are partially related. From the ChIP-Seq dataset, a total of 80 putative S-HsfA2 targets were identified (Supplemental Figure S4C), 65 of which contained the HRE (Supplemental Table S1).

We next confirmed the binding of S-HsfA2 or tDBD to the HRE. The bacterially expressed and purified glutathione S-transferase (GST)-tagged S-HsfA2 fusion protein (GST-S-HsfA2) (Supplemental Figure S5) was used in electrophoretic mobility shift assays (EMSAs). The results showed that GST-S-HsfA2, but not the mock control (GST alone), specifically bound to HRE *in vitro* (Figure 2A). According to the yeast one-hybrid (Y1H) assay, S-HsfA2 also specifically recognized HRE (Figure 2B). Interestingly, His6-tDBD recognized the HRE, but His6-DBD bound to the HSE *in vitro* (Figure 2C). Consistent with this observation, His-tagged HsfA2 did not bind to HRE *in vitro* (Supplemental Figure S6). These findings indicate that S-HsfA2 uses the tDBD to bind to HREs *in vitro*.

HRE serves as a heat response element

To determine the heat induction effect of HRE, we constructed an HRE trimer driving the minimal 35S promoter (-46/+8, 35Sm)-β-glucuronidase (*GUS*) reporter gene (*HRE-35Sm:GUS*) in transgenic *Arabidopsis* (Figure 3A). HRE could drive 35Sm to enable clear GUS histochemical staining in seedlings. However, as observed for the vector control (*35Sm:GUS*), mutations in the HRE (*mHRE-35Sm:GUS*) caused a full loss of GUS staining regardless of heat stress. Weak GUS signals were mainly detected

in the shoot apical region and the shoot vascular system in the *HRE-35Sm:GUS* seedlings. In a time-course study, GUS signals were enhanced under heat stress (37°C) for 15-30 min, suggesting that GUS might be transported *via* the vascular system from the shoot apical region to the shoot to respond to the heat response at the whole-plant level.

A quantitative GUS expression assay at both the mRNA (Figure 3B) and protein (Figure 3C) levels revealed that HRE conferred heat responsiveness to 35Sm by 2- to 4-fold. This heat responsiveness was also heat (37°C)-time dependent (Figure 3D). HRE-bound nuclear extracts were derived from *Arabidopsis in vitro*, particularly from extreme heat shock (42°C)-treated *Arabidopsis* nuclear extracts (Figure 3E), further suggesting that HRE has the biochemical characteristics of a heat response element. Overall, the above molecular, biochemical, and genetic data strongly demonstrated that the HRE serves as a heat response element.

S-HsfA2 acts as an HRE-binding transcription repressor in *Arabidopsis*

To determine whether S-HSfA2 depends on the HRE to regulate a gene, we introduced the *35S:S-HsfA2-Flag* or *35S:S-HsfA2$^{L\text{-}A}$-Flag* effector into the *HRE-35Sm:GUS* reporter lines by crossing, and we found that GUS protein levels were downregulated compared with those in uncrossed controls (Figure 3F). In contrast, the *35S:S-HsfA2$^{L\text{-}A}$-Flag* effector increased GUS levels (Figure 3F). These results confirmed that S-HsfA2 is an HRE-binding transcription repressor. This finding also indicated that the LxLxLx motif within the LRD is needed for S-HsfA2 repression activity in plant cells, which is consistent with findings in yeast cells (Supplemental Figure S1).

S-HsfA2, S-HsfA4c, and S-HsfB1 represent new kinds of plant HSF

Given that S-HsfA2 is an HRE-binding transcriptional repressor and confers extreme heat sensitivity in *Arabidopsis*, we hypothesized that S-HsfA2 represents a

new HSF. The new HSFs are not limited to S-HsfA2 because tDBD is responsible for HRE binding and is highly conserved among S-HSFs. To provide further supporting data, we characterized S-HsfA4c, S-HsfB1, and S-HsfB2a, which were previously identified (Liu et al., 2013).

HsfA4c (At5G45710) has two splice variants (Liu et al., 2013): an intron 2-containing predominant S-*HsfA4c* and a less abundant intron 1-containing full-length *HsfA4c*. *S-HsfA4c* encodes S-HsfA4c. *S-HsfA4c* was constitutively expressed, but heat stress enhanced its expression (Figure 4A). S-HsfA4c shares similar structural features (LxLxLx motif-containing LRD, Figure 4A) with S-HsfA2. S-HsfA4c acted as a transcriptional repressor in yeast cells, and LRD was needed for its transcriptional repression (Supplemental Figure S7). S-HsfA4c bound to the HRE according to both Y1H (Figure 4B) and electrophoretic mobility shift assays (EMSAs) (Figure 4C). Overexpression of *35S:S-HsfA4c-GFP* (S-HsfA4c-OE) resulted in heat sensitivity compared with that of the *35S:GFP* vector control (Figure 4D), whereas T-DNA insert-mediated knockdown of *S-HsfA4*c together with *HsfA4c* increased thermotolerance (Figure 4E). Interestingly, heat stress enhanced the translocation of HsfA4c-GFP into the nucleus (Figure 4F), similar to what was observed for S-HsfA2-GFP (Supplemental Figure S3).

Like *S-HsfA4c*, *S-HsfB1* was constitutively expressed, but heat stress strongly increased its expression (Figure 5A). In contrast, *S-HsfB2a* was heat stress inducible (Figure 5A). S-HsfB1 and S-HsfB2a were localized to the nucleus of plant cells (Figure 5B). S-HsfB2a is a weak transcriptional activator in yeast cells, but S-HsfB1 has no transactivation activity (Supplemental Figure S8). According to the Y1H results, both S-HsfB1 and S-HsfB2a could bind to the HRE (Figure 5C). However, S-HsfB1, but not S-HsfB2a, bound to the HRE *in vitro* (Figure 5D). Thus, S-HsfB2a did not appear to be an HRE-binding protein. Therefore, we selected S-HsfB1 for further confirmation of its effects on *Arabidopsis* thermotolerance. We found that

seedling survival, especially chlorophyll content, was markedly reduced by S-HsfB1 overexpression (*35S:S-HsfAB1-RFP*) in *Arabidopsis* plants under heat stress (Figure 5E). In contrast, the specific knockdown of *S-HsfB1* through antisense RNA (targeting the retained intron sequences) and both the *HsfB1* and *S-HsfB1* double knockout resulted in increased seedling survival, especially in terms of the chlorophyll content, under heat stress (Figure 5F). Collectively, these data indicate that HRE binding and negative regulatory effects on extreme heat stress tolerance are common for S-HsfA2, S-HsfA4c, and S-HsfB1. Therefore, we conclude that these three S-HSFs represent new kinds of plant HSFs.

The HRE-HRE-like element is involved in heat induction of the *HSP17.6B* promoter

Using S-HsfA2 as a representative S-HSF, we further investigated the transcriptional cascades linking S-HsfA2 to *Arabidopsis* heat tolerance sensitivity. Among the 80 putative targets of S-HsfA2, we focused on the heat shock-induced small *HSP* gene *HSP17.6B* (At2G29500) (Scarpeci et al., 2008). By searching the ChIP-Seq dataset, we identified the 103-bp promoter region of *HSP17.6B*. This region contains 14-bp DNA sequences (5′-GAAGAAGGAAGAAC-3′, -540 to -527 relative to the transcription start site), which consists of one perfect HRE (5′-GAAGAAG-3′) and one HRE-like (5′-GAAGAAC-3′), named the HRE-HRE-like element (Figure 6A). HSP17.6Bp also contains an HSE (5′-aTTCtaTTCaaTTCa-3′).

To determine the role of the HRE-HRE-like element in the response of HSP17.6Bp to heat stress, we generated transgenic *Arabidopsis* lines harboring HSP17.6Bp or HSP17.6Bp lacking the HRE-HRE-like element (HSP17.6BpΔHRE), which drives *GUS* reporter expression. GUS histochemical staining revealed a specific heat-induced expression pattern of HSP17.6Bp, and GUS signals were detected in the shoot apical region and the shoot vascular system after heat stress. Further quantitative GUS protein expression showed that HRE-HRE-like deletion did not change the

heat-inducible expression pattern of HSP17.6Bp but did affect the heat-induced expression level (increased at 37°C but largely decreased at 42°C) (Figure 6B). These results suggested that the HRE-HRE-like element is involved in the heat induction of HSP17.6Bp, especially under heat shock at 42°C.

S-HsfA2 negatively regulates *HSP17.6B* by binding to the HRE-HRE-like element

ChIP–qPCR assays verified the binding of S-HsfA2 to the HRE-HRE-like-containing HSP17.6Bp region (Figure 6C). Correspondingly, the heat-induced expression of *HSP17.6B* was upregulated in the *S-HsfA2*-knockdown lines but downregulated in the *S-HsfA2*-overexpressing lines (Figure 6D). These results indicated that S-HsfA2 negatively regulates *HSP17.6B* by directly binding to the HRE-HRE-like element within HSP17.6Bp.

HSP17.6B* confers heat tolerance in *Arabidopsis

We next tested whether *HSP17.6B* is involved in thermotolerance. We obtained two T-DNA-inserted *HSP17.6B* mutants (*hsp17.6b-1* and *hsp17.6b-2*), *35S:HSP17.6B-Flag* transgenic *Arabidopsis* plants in the WT background (HSP17.6B-OE), and *35S:HSP17.6B-Flag* transgenic *Arabidopsis* plants in the *hsp17.6b-1* background (HSP17.6B-KI) (Figure 7A). Subsequent heat tolerance phenotype analyses revealed that two *hsp17.6b* mutants were heat sensitive, whereas the HSP17.6B-OE lines were heat tolerant (Figure 7B). The heat tolerance of the HSP17.6B-KI lines was similar to that of the WT control (Figure 7C), suggesting that expressing *35S:HSP17.6B* rescued the heat-sensitive phenotype of the *hsp17.6b* mutant.

Overall, *HSP17.6B* confers thermotolerance, but S-HsfA2 represses *HSP17.6B* *via* the HRE-HRE-like element, which is involved in heat induction by Hsp17.6Bp. Thus, *HSP17.6B* links S-HsfA2 to extreme heat sensitivity in *Arabidopsis*. Based on

these findings, we propose that a noncanonical HSR is involved in extreme heat sensitivity, *i.e.*, S-HsfA2-HRE-*HSP17.6B.*

***HSP17.6B* overexpression mediates heat tolerance hyperactivation**

We noted that *HSP17.6B* overexpression also retarded seedling growth under normal conditions, as indicated by both decreased biomass (fresh weight) and low chlorophyll content (chlorosis) (Figure 8 A). When grown in soil, the HSP17.6B-OE seedlings exhibited a dwarf but heat-tolerant phenotype (Figure 8 B). These results demonstrated that *HSP17.6B* overexpression mediated heat tolerance hyperactivation. Therefore, the noncanonical S-HsfA2-HRE-*HSP17.6B* HSR can contribute to attenuating heat tolerance hyperactivation.

Canonical HSR: HsfA2-HSE-*HSP17.6B*

HSP17.6Bp also contains an HSE, suggesting that *HSP17.6B* is regulated by HSFs. It has been reported that the constitutive expression of *HSP17.6B* is activated by *HsfA2* overexpression, but the heat-induced expression of *HSP17.6B* is markedly reduced in the *HsfA2* knockout mutant, suggesting that *HSP17.6B* is a putative target of HsfA2 (Nishizawa et al., 2006). ChIP–qPCR using *Arabidopsis* transiently expressing *35S:HsfA2-RFP* with an anti-RFP antibody showed the direct binding of HsfA2-RFP to the HSE-containing *HSP17.6Bp* region (Supplemental Figure S9A, B). According to the Y1H assay, HsfA2 also bound to the HSE within HSP17.6Bp (Supplemental Figure S9C). Together with the findings of a previous report (Nishizawa et al., 2006), our data confirmed that *HSP17.6B* is a direct target of HsfA2. Thus, a canonical HSR (HsfA2-HSE-*HSP17.6B*) is suggested.

Taken together, the above data indicate that S-HsfA2 and HsfA2 have opposite effects on *HSP17.6B* expression: repression by S-HsfA2 but activation by HsfA2. These findings suggested that the balance between HsfA2 and S-HsfA2 activity serves

to fine-tune the *HSP17.6B* expression level, possibly preventing the hyperactivation of heat tolerance mediated by HSP17.6B overexpression.

S-HsfA2 interacts with several HSFs, including HsfA2

S-HSFs can negatively regulate the activities of HSFs through protein–protein interactions (Wu et al., 2019; Zhang et al., 2024). We therefore explored whether and how S-HsfA2 regulates the activities of HSFs, especially HsfA2, through protein–protein interactions. To address this issue, we first used a yeast two-hybrid (Y2H) assay to screen *Arabidopsis* HSFs that interact with S-HsfA2. The results showed that S-HsfA2 interacted with HsfA1e, HsfA2, HsfA3, HsfA7a, and HsfB2b among the 19 *Arabidopsis* HSFs tested (Figure 9A). In this study, we focused on HsfA2. GST pulldown confirmed the interaction between S-HsfA2 and HsfA2 *in vitro* (Figure 9B). Importantly, Y2H and bimolecular fluorescence complementation (BiFC) assays revealed that S-HsfA2 interacted with the DBD of HsfA2 (Figure 9C, 9D), which is consistent with previous findings that S-ZmHsf17 can interact with the DBD of full-length ZmHsf17 in a Y2H assay (Zhang et al., 2024).

S-HsfA2 decreases the HSE-binding capacity of HsfA2 *in vitro*

The streptavidin-bead pulldown assay is an efficient *in vitro* method for evaluating the DNA binding capacity of transcription factors (Deng et al., 2003). Because of the specific interaction between His6-HsfA2 and GST-S-HsfA2 *in vitro* (Figure 9B), we used His6-HsfA2 and GST-S-HsfA2 in this pulldown assay (Figure 10A). The results showed that His6-HsfA2 prebinding with GST-S-HsfA2 decreased the signal intensity of the biotin-labelled HSE bait-binding His6-HsfA2 (Figure 10A). These findings suggest that S-HsfA2 serves as a negative binding regulator of HsfA2 to decrease the HSE-binding capacity of HsfA2 *in vitro*.

S-HsfA2 attenuates HsfA2-regulated *HSP17.6B* promoter expression

We then explored the effects of S-HsfA2, a negative binding regulator of HsfA2, on HsfA2-mediated HSP17.6Bp expression. Based on the interaction between HsfA2-nYFP and S-HsfA2-cYFP in the BiFC assay (Figure 9D), we used dual-luciferase (LUC) reporter assays to test whether S-HsfA2-cYFP inhibits the *HSP17.6Bp* activity activated by HsfA2-nYFP. To avoid the effect of S-HsfA2 on *HSP17.6Bp*, a short, truncated 135-bp *HSP17.6Bp* (sHSP17.6Bp) containing HSE but lacking an HRE-HRE-like sequence was used in this assay. Compared with the GUS effector controls, HsfA2-nYFP increased *sHSP17.6Bp-LUC* reporter expression in tobacco cells. As expected, S-HsfA2-cYFP failed to regulate sHSP17.6Bp. However, compared with the GUS-cYFP control, S-HsfA2-cYFP reduced the HsfA2-nYFP-mediated *sHSP17.6Bp-LUC* reporter expression level by more than 50% (Figure 10B). These results establish the importance of S-HsfA2 in HsfA2-regulated HSP17.6Bp expression by preventing HsfA2 from binding to the HSE.

Discussion

The AS events of HSFs have been extensively described in plants (Sugio et al., 2009; Liu et al., 2013; Cheng et al., 2015; Wu et al. 2019; Ma et al., 2023; Zhang et al., 2024), but the specific biological functions of these splice variants and their underlying regulatory mechanisms have largely not been determined. In this study, we demonstrated that *Arabidopsis* S-HSFs, *i.e.*, S-HsfA2, S-HsfA4c, and S-HsfB1, derived from HSF splicing variants represent new kinds of HSF. Several molecular and genetic studies support this conclusion: (*i*) S-HSFs are localized in the nucleus, especially after heat stress, reflecting their cellular heat response features; (*ii*) S-HSFs have a unique conserved tDBD that binds to the HRE, a new heat response element; and (*iii*) S-HSFs confer extreme heat stress sensitivity as negative regulators of heat tolerance. Using S-HsfA2 as a representative S-HSF, we further revealed the molecular mechanisms underlying the ability of S-HSFs to prevent canonical HSR hyperactivation caused by *HSP17.6B* overexpression. Therefore, our findings reveal a

novel mechanism by which plants balance thermotolerance and growth and offer insight into the breeding of thermotolerant plants.

Splice variants of HSFs generate new plant HSFs

In this work, we showed that *Arabidopsis* S-HsfA2, S-HsfA4c, and S-HsfB1 are generated from partial or full retention of the conserved intron in the DBD. S-HSFs (such as S-HsfA2, S-HsfA4c, and S-HsfB1) lack all the C-terminal functional domains of HSFs but share a common unique structural feature, *i.e.*, tDBD. Another structural feature of S-HSFs is extended motifs or domains encoded by the retained introns. However, their lengths and sequences vary among different S-HSFs and are therefore less conserved than those of the tDBD. For example, lengths of 26 aa, 30 aa, and 13 aa were found for S-HsfA2, S-HsfA4c, and S-HsfB1, respectively. We found that the extended domain, *i.e.*, the LRD, allows S-HsfA2 to act as a transcriptional repressor. More importantly, LRD is needed for the functions of S-HsfA2 in heat tolerance regulation. Therefore, we concluded that the extended motifs or domains are essential for the functions of S-HSFs.

Although S-HsfA2, S-HsfA4c, and S-HsfB1 only have conserved tDBD sequences plus adjacent extended motifs or domains, these small HSF isoforms are of biological importance since they negatively regulate extreme heat tolerance in *Arabidopsis*. Notably, two aspects related to heat stress are consistent with their biological relevance. First, *S-HsfA2*, *S-HsfA4c*, and *S-HsfB1* strongly respond to extreme heat stress, indicating that they function in extreme heat stress in *Arabidopsis.* We also found that the constitutive expression of S-HsfA2 inhibits *Arabidopsis* growth. Considering this, *Arabidopsis* plants do not produce S-HSFs or produce fewer S-HSFs under normal conditions to avoid growth inhibition. Another is the heat stress-induced translocation of S-HsfA2 and S-HsfA4c into the nucleus to regulate target gene transcription. Overall, our data strongly support that S-HSFs act as new kinds of HSFs and thus increase the diversity of HSFs.

Surprisingly, AS events in the DBD of plant HSFs have not been detected in animal HSFs. Several reports have shown that animal HSFs utilize exon skipping to generate HSF splicing isoforms containing full-length DBDs (Tanabe et al., 1999; Fujikake et al., 2005; Zhang et al., 2010; Neueder et al., 2014). These animal HSF isoforms have different transcriptional activities and work synergistically to regulate the transcription of *HSPs* (Tanabe et al., 1999; Neueder et al., 2014). Therefore, new kinds of HSF seem to be plant specific, reflecting a unique feature of plant systems.

HRE is a heat response element

HSE is a known heat-responsive element and is essential for heat-inducible transcription of genes. In this study, we showed that the HRE is a heat response element, as determined by molecular, biochemical, and genetic analyses. HRE confers a minimal promoter response to heat and is responsible for heat-induced expression of the *HSP17.6B* promoter. He et al. (2022) reported a heat stress sensing and transmission pathway at the whole-plant level. Nitric oxide (NO) bursts in the shoot apex under heat stress, and NO, an S-nitrosoglutathione, can rapidly move from shoot to root through the vascular system in whole *Arabidopsis* plants. Interestingly, the GUS reporter driven by HREs was constitutively expressed in the shoot apical region, and heat stress enhanced and promoted GUS movement along the shoot vascular system to the leaves and hypocotyl. Therefore, the HRE exhibits heat stress sensing and transmission patterns, indicating a heat regulation function.

The HRE consists of two inverted HSE blocks (nGAAn) that share a G base. Although HRE is partially related to HSE, it does not bind to the DBD or to HsfA2 *in vitro*. In contrast, HRE is recognized by tDBD, S-HsfA2, S-HsfA4c, and S-HsfB1 *in vitro*. Loss of the wing domain within the DBD might partly explain why the DNA-binding characteristics of the tDBD change.

We also noted that HRE can drive the constitutive expression of the *GUS* reporter and bind nuclear extracts under normal conditions. These data suggest that some

unknown constitutive transcription factors other than S-HSFs exist in *Arabidopsis*. In the future, these HRE-binding transcription factors need to be screened by Y1H and DNA–protein pulldown assays. These studies can further characterize the working molecular mechanisms of HRE.

The noncanonical HSR: S-HsfA2-HRE-*HSP17.6B*

Using S-HsfA2 as a representative S-HSF, we proposed the S-HsfA2-HRE-*HSP17.6B* noncanonical HSR. In this HSR, S-HsfA2 binds to the HRE-HRE-like element to prevent *HSP17.6B* overexpression and eventually attenuates *Arabidopsis* tolerance to extreme heat. Given that *HSP17.6B* overexpression-mediated heat tolerance hyperactivation represses *Arabidopsis* growth, our results underscore the biological significance of this noncanonical HSR: preventing plant heat tolerance hyperactivation to maintain proper growth. Although we propose a noncanonical HSR based on S-HsfA2, S-HSF-mediated noncanonical HSRs should constitute a widespread regulatory mechanism in planta because the tDBD is highly conserved in S-HSFs and because the HRE can be bound by the tDBD.

S-HSFs act as new negative binding regulators of HSFs

During the canonical HSR, cells often utilize negative binding regulators of HSFs, including HSP70 and HSF-binding proteins (HSBPs), to inactivate HSFs in different ways (Morimoto, 1998). HSP70 represses the transcriptional activity of HSFs by directly binding to the transcriptional activation domain (Baler and Voellmy, 1996). HSBPs are conserved small nuclear proteins that dissociate trimeric HSFs and abate transcription activation (Satyal et al., 1998). *Arabidopsis* HSBP (AT4G15802) attenuates the canonical HSR by interacting with HSFs and decreasing HSF DNA-binding activity (Hsu et al., 2010). S-ZmHsf17 can interact with the DBD of ZmHsf17 to suppress the transactivation of ZmHsf17 by reducing the HSE-binding capacity of ZmHsf17 (Zhang et al., 2024), suggesting that S-HSFs may act as negative binding regulators of HSFs. In the present study, S-HsfA2 was also identified as a

negative binding regulator of HsfA2. Unlike HSP70 and HSBPs, S-HsfA2 binds to the DBD, thus decreasing the HSE-binding capacity of HSFs such as HsfA2 and eventually attenuating HsfA2-regulated *HSP17.6B* promoter activity. According to the Y2H results, S-HsfA2 interacts with five HSFs (HsfA1e, HsfA2, HsfA3, HsfA7a, and HsfB2b). It is of interest to explore whether S-HsfA2 inactivates HsfA1e, HsfA3, HsfA7a, and HsfB2b.

S-HsfA2 molecular working model

Taken together, our findings in this study support the use of a molecular model in which S-HsfA2 balances the gain and loss of canonical HsfA2-regulated *HSP17.6B* overexpression-mediated HSR hyperactivation. S-HsfA2 directly binds to the HRE of the *HSP17.6B* promoter to repress *HSP17.6B* expression and interacts with the DBD of HsfA2 to inactivate HsfA2 binding to the *HSP17.6B* promoter, ultimately alleviating hyperactivation of the HsfA2-HSE-*HSP17.6B* HSR (Figure 11). Considering that S-HsfA2 generation occurs upon exposure to severe heat, this negative regulatory pathway is not an “enemy” but rather a “friend” to avoid canonical HSR hyperactivation in *Arabidopsis*.

Our findings could lead to the breeding of thermotolerant plants

It has been reported that natural variation in *HsfA2* pre-mRNA splicing is associated with changes in thermotolerance during tomato domestication (Hu et al., 2020). In the present study, selective knockdown of S-HsfA2 improved the tolerance to transient extreme heat (45°C for 2 h). Given that S-HsfA2 favours *Arabidopsis* growth under extreme temperature conditions by inhibiting heat tolerance hyperactivation mediated by HSP17.6B overexpression, our findings offer insights for plant breeding to orchestrate plant extreme heat (such as heat waves) tolerance and growth via extreme heat-specific expression of *S-HsfA2* homologues.

Materials and methods

Plant Materials and Growth Conditions

Arabidopsis (*A. thaliana*, Columbia-0), the *hsfa4c-1* mutant (SALK_016087C), the *hsfa4c-2* mutant (SALK_138256C), *hsp17.6b-1* (SALK_013435C), *hsp17.6b-2* (WISCDSLOXHS008_12D), and *hsfb1* (SALK_104713C) were surface sterilized with sodium hypochlorite (25%, v/v) and washed with sterile double distilled water. After vernalization treatment for 3 days, the seeds were grown on half Murashige and Skoog (MS) agar plate media with a 16-h/8-h light/dark cycle at 22°C and a white light intensity of 150 mmol m^{-2} s^{-1}. In this study, the age of seedlings was calculated as days after sowing (DAS).

Primers

The primers and synthesized oligonucleotides used in this study are listed in Supplemental Table S2.

Recombinant plasmid construction

The target DNA fragments were obtained by PCR with the Taq enzyme (Takara, Japan) and subsequently cloned and inserted into the corresponding vectors with the ClonExpress II One Step Cloning Kit (Vazyme Biotech, Nanjing, China).

The S-HsfA2 and S-HsfA2$^{L\text{-}A}$ coding sequences lacking stop codons were amplified from *Arabidopsis* genomic DNA using S-HsfA2-Flag-F/-R and S-HsfA2-Flag-F/S-HsfA2mut-Flag-R, respectively. Similarly, the coding sequence of *HSP17.6B* lacking the stop codon "TGA" was amplified using HSP17.6B-Flag-F/-R. The PCR products were cloned and inserted into the *Xba*I/*Bam*HI site *35S:3×Flag* (our laboratory) and sequenced using GUS-R to generate *35S:S-HsfA2-Flag* (S-HsfA2-OE), *35S:S-HsfA2$^{L\text{-}A}$-Flag* (S-HsfA2$^{L\text{-}A}$-OE), and *35S:HSP17.6B-Flag* (HSP17.6B-OE).

We used a fusion PCR method to generate the *35S:S-HsfA2-RNAi* construct based on pUCCRNAi. First, the PCR1 products (forward intron 1a of *HsfA2*, 104 bp) were amplified from the BD-S-HsfA2 plasmid using the primers F1/R1. Second, the

PCR2 products (intron 1 of potato GA20 oxidase, 219 bp) were amplified from pUCCRNAi using the primers F2/R2. Third, the PCR3 products (reverse intron 1a of *HsfA2*, 105 bp) were amplified from the BD-S-HsfA2 plasmid using the primers F3/R3. Fourth, fusion PCR was performed in a total volume of 50 μL containing 33 ng of each purified PCR product (template) for 5 cycles at an annealing temperature of 55°C (without primers) followed by 25 cycles (adding F1/R3) at 65°C. The fusion fragments were cloned and inserted into the *Bam*HI/*Sac*I site of pBI121 and sequenced using GUS-R.

For the expression vector constructs, HsfA2-RFP-F/-R, S-HsfB1-RFP-F/-R and S-HsfB2a-RFP-F/-R were used to amplify the coding regions of HsfA2, S-HsfB1 and S-HsfB2a from cDNA, which were subsequently cloned and inserted into the *Bam*HI/*Spe*I sites of pCAMBIA1300. The resulting *35S:HsfA2-RFP*, *35S:S-HsfB1-RFP and 35S:S-HsfB2a-RFP* were sequenced using RFP-R. The expression vectors *35S:S-HsfB1* and *35S:S-HsfB2a* were constructed by antisense RNA knockdown technology and reverse primers anti-S-HsfB1-F/-R and anti-S-HsfB2a-F/-R. The coding region of S-HsfA4c lacking the stop codon TAG was amplified from cDNA using the primers S-HsfA4c-GFP-F/-R and cloned and inserted into the *Bgl*II/*Spe*I sites of pCAMBIA1302 (Clontech) to generate *35S:S-HsfA4c-GFP*. The coding region of S-HsfA2 lacking the stop codon TAG was amplified from genomic DNA using the primers S-HsfA2-GFP-F/-R and cloned and inserted into the *Nco*I/*Spe*I sites of pCAMBIA1302 (Clontech) to generate *35S:S-HsfA2-GFP*.

For the AD constructs, the coding sequences of 19 HSFs, S-HsfA2, and S-HsfA4c were amplified from heat-treated *Arabidopsis* cDNA using the corresponding primers, inserted into the *Bam*HI/*Bgl*II site of pGAD424 (Clontech) to generate corresponding AD-HSF fusion vectors and identified by sequencing.

For bait construction, 3×HRE, 3×mHRE, HSE (Enoki and Sakurai, 2011), and mHSE were synthesized by Shanghai Sangon Biotechnology and subsequently cloned

and inserted into pHIS2.1 (Clontech). The PCR products were cloned and inserted into the *Eco*RI/*Spe*I site of the pHIS2.1 vector (Clontech) and sequenced using pHIS2.1 forward or reverse primers.

For the BD constructs, the S-HsfA2 and S-HsfA2^{L-A} coding sequences were amplified from *Arabidopsis* genomic DNA using BD-S-HsfA2-F/-R and BD-S-HsfA2-F/BD-S-HsfA2mut-R, respectively. The S-HsfA4c, S-HsfA4c△LRD, S-HsfB1 and S-HsfB2a coding sequences were amplified from cDNA using BD-S-HsfA4c-F/-R, BD-S-HsfA4c-F/BD-S-HsfA4cΔLRD-R, BD-S-HsfB1-F/-R and BD-S-HsfB2a-F/-R, respectively. The corresponding PCR products were subsequently cloned and inserted into the *Eco*RI/*Pst*I sites of pGBKT7 (Clontech) to generate the BD-S-HsfA2, BD-S-HsfA2^{L-A}, BD-S-HsfA4c, BD-S-HsfA4cΔLRD, BD-S-HsfB1 and BD-S-HsfB2a constructs. T7 primers were used to sequence the BD fusion vectors.

To generate the glutathione S-transferase (GST)-tagged expression plasmid pGEX4T-S-HsfA2. Using the BD-S-HsfA2 plasmid as a template, the PCR product was amplified with GST-S-HsfA2-F/-R and subsequently cloned and inserted into the *Bam*HI/*Sal*I sites of pGEX-4T.

For the His6-tagged expression plasmids, the HsfA2, S-HsfA2, S-HsfA4c S-HsfB1 and S-HsfB2a coding sequences were amplified from cDNA using His6-HsfA2-F/-R, His6-HsfA2-F/His6-S-HsfA2-R, His6-S-HsfA4c-F/-R, His6-S-HsfB1-F/-R and His6-S-HsfB2a-F/-R, respectively. The PCR products were inserted into the *Bam*HI/*Sal*I sites of pET-28a(+) to generate His6-HsfA2, His6-S-HsfA2, His6-S-HsfA4c, His6-S-HsfB1 and His6-S-HsfB2a. Then, using His6-HsfA2 and His6-S-HsfA2 as templates, the DBD and tDBD coding sequences were amplified with His6-DBD-F/-R and His6-DBD-F/His6-tDBD-R. The PCR products were also cloned and inserted into the *Bam*HI/*Sal*I sites of pET-28a(+) to obtain His6-DBD and His6-tD. The plasmids were subsequently sequenced using the T7 primer.

We used an asymmetric overlap extension PCR method to construct the *HRE-35Sm:GUS* and *mHRE-35Sm:GUS* plasmids using 3×HRE-35Sm-F or 3×mHRE-35Sm-F and the common reverse primer HRE-35Sm-R. The PCR products were subsequently cloned and inserted into the *Hin*dIII/*Xba*I sites of pBI121 instead of the 35S promoter. The recombinant reporter plasmids were subsequently sequenced using GUS-R primers for validation.

The wild-type *HSP17.6B* promoter (HSP17.6Bp, -637/+1) and HSP17.6BpΔHRE were amplified from *Arabidopsis* genomic DNA using HSP17Bp-F/-R and HSP17BpΔHRE-F/-R, respectively. The above PCR products were cloned and inserted into the *Hin*dIII/*Bam*HI sites of pBI121 and sequenced by GUS-R to generate the corresponding constructs *HSP17.6Bp:GUS* and *HSP17Bp*ΔHRE*:GUS.*

A short, truncated 135-bp *HSP17.6B* promoter fragment (sHSP17.6Bp) was amplified from *Arabidopsis* genomic DNA using sHSP17.6Bp-LUC-F/-R and inserted into the *Hin*dIII/*Spe*I sites of pGreenII0800-LUC (LUC vectors containing the REN gene under the control of the 35S promoter as an internal control) to generate the reporter vector *sHSP17.6Bp:LUC.*

For the BiFC constructs, the coding regions of S-HsfA2 and HsfA2 and a series of HsfA2 genes progressively truncated from the N-terminus were amplified from AD-S-HsfA2 and AD-HsfA2 using cYFP-S-HsfA2-F/-R, nYFP-HsfA2-F/-R, nYFP-HsfA2ΔN-F and nYFP-HsfA2ΔNΔDBD-F, respectively. The above PCR products were cloned and inserted into the *Xba*I/*Bam*HI sites of modified pCAMBIA1300 containing the cYFP or nYFP coding sequence to generate the corresponding constructs S-HsfA2-cYFP, HsfA2-nYFP, HsfA2ΔN-nYFP, and HsfA2ΔN-DBD-nYFP. The above vectors were identified by sequencing nYFP-R or cYFP-R.

Plant transformation and crossing

A series of plasmids related to S-HsfA2 (*35S:S-HsfA2-Flag*, *35S:S-HsfA2$^{L\text{-}A}$-Flag*, and *35S:S-HsfA2-RNAi*), GUS reporter constructs [*HRE-35Sm:GUS*, *mHRE-35Sm:GUS*, and *35Sm:GUS* (Wang et al., 2023)], recombinant vectors for HSP17.6B (*35S:HSP17.6B-Flag*, *HSP17.6Bp:GUS*, and *HSP17Bp*Δ*HRE:GUS*), and GFP fusion vectors (*35S:S-HsfA2-GFP* and *35S:S-HsfA4c-GFP*) were introduced into the *Agrobacterium* GV3101 strain, which was subsequently used to transform the Columbia wild type using the flower infiltration method. The transgenic plants used in this study were T_3 homozygous plants. The transgenic plants used in this study were T_3 homozygous plants.

35S:HsfA2-RFP was subsequently introduced into *A. tumefaciens* GV3101. Ten-day-old *Arabidopsis* plants were vacuum infiltrated with *A. tumefaciens* as described by Marion et al. (2008) and subsequently incubated for 3 days.

The effector lines (♂,*35S:S-HsfA2-Flag*, *35S:S-HsfA2$^{L\text{-}A}$-Flag*) were crossed with GUS reporter lines (♀, *HRE-35Sm:GUS*) to generate T_1 seeds by artificial pollination. To select the positive crossing lines, the leaves of T1 seedlings of the crossing lines (+effector) and control lines (−effector) were subjected to PCR analysis using a genomic DNA template. The following primers were used: S-HsfA2-F/121-R. Leaves from ten independent positive-crossing lines were used for protein isolation. *GUS* expression was detected by Western blotting as described below.

Subcellular localization

For S-HsfA2 and S-HsfA4c localization in *Arabidopsis* cells, the roots of 7-day-old *35S:S-HsfA2-GFP* and *35S:S-HsfA4c-GFP* transgenic *Arabidopsis* plants were observed via fluorescence microscopy and laser confocal microscopy (SP8) in the GFP channel. Cell nuclei were stained with 4,6-diamidino-2-phenylindole (DAPI, C0060; Solarbio). The fusion protein expression vectors *35S:S-HsfB1-RFP* and *35S:S-HsfB2a-RFP* were transiently transformed into tobacco. After 48 h, the leaf cells

were stained with the nuclear stain DAPI under a fluorescence microscope in the RFP channel.

Transcriptional activity assay in yeast cells

The transcriptional activation activity was determined in synthetic defined (SD) medium lacking Trp but containing 40 μg mL^{-1} 5-bromo-4-chloro-3-indolyl-α-D-galactopyranoside (X-α-gal; Sigma–Aldrich) at 30°C for 3 days. BD and BD-PVERF15 were used as negative and positive controls, respectively. The β-galactosidase activity in liquid cultures was determined using an o-nitrophenyl-β-D-galactopyranoside (ONPG) assay in three independent clones.

GUS staining

GUS reporter transgenic *Arabidopsis* plants were immersed in precooled 90% [v/v] acetone for 20 min and then soaked in GUS staining solution (0.5 mg/mL X-Gluc, 100 mM Na_3PO_4 [pH=7.0], 50 μM $K_4[Fe_6]\cdot 3H_2O$, 50 μM $K_3[Fe_6]$, 1 mM EDTA [pH=8.0]) at 37°C in the dark for 12 to 24 h. After elution with 100% [v/v] anhydrous ethanol several times, observations were made with a microscope.

Heat stress treatments

In a thermotolerance test, *Arabidopsis* plants (10 or 12 DAS) were incubated at 45°C for 2 h following recovery at 22°C for 5 or 15 days. In the soil experiments, plants (12 DAS) were planted in soil for 8 days, treated in an incubator at 45°C for 3 h and returned to 22°C for 5 days.

To prepare nuclear extracts, 14-day-old *Arabidopsis* plants were transferred to filter paper with 1/4 MS liquid media and subjected to heat shock in a temperature incubator (22°C, 37°C, and 42°C) for 1 h.

To analyse GUS mRNA or protein expression levels, 14-day-old *HRE-35Sm:GUS*, m*HRE-35Sm:GUS,* or *35Sm:GUS* transgenic *Arabidopsis* plants

were subsequently transferred to filter paper in 1/4 MS liquid media and subjected to heat shock in a temperature incubator (22°C, 37°C, and 42°C) for 1 h. For heat time-course analysis of the *HRE-35Sm:GUS* transgenic *Arabidopsis* plants, samples were taken at various treatment intervals (0, 15, 30, 45, and 60 minutes).

Heat tolerance assays

For the survival rate, the true leaves of the plants were chlorotic and considered dead. For the root length assay, the seeds of WT and transgenic *Arabidopsis* plants (*i.e.*, S-HsfA2-OE, S-HsfA2$^{L\text{-}A}$-OE, and S-HsfA2-KD) were sown on vertical one-half-length MS agar plates at 22°C for 12 days and then subjected to root length analysis with the ImageJ analysis tool. The detached shoots were subjected to chlorophyll content analysis. Shoot chlorophyll contents were determined at 663 and 645 nm as described previously (Chen et al., 2024).

RNA isolation, cDNA synthesis and PCR analysis

Total RNA was extracted from plant materials using an RNAprep Pure Plant Kit with on-column DNase digestion (Tiangen Biotech, China) according to the manufacturer's protocol. First-strand cDNA was synthesized from RNA (approximately 2 μg) with oligo(dT) primers according to the instructions of the PrimeScript First Strand cDNA Synthesis Kit (Takara).

RT–PCR splicing analysis was carried out with Ex-Taq polymerase (Takara, Japan) for a total of 25-28 cycles. *YLS8* (AT5G08290) was used as a loading control.

RT–qPCR was performed on an IQ5 Multicolor Real-Time PCR Detection System (Bio-Rad) with the SYBR Premix Ex-Taq Kit (Takara). *EF-1α* (AT1G18070) was used as an internal control. The relative expression levels were analysed using the delta-delta cycle threshold method according to CFX Manager™ software. A P value < 0.05 indicated a statistically significant difference.

Chromatin immunoprecipitation combined with high-throughput sequencing (ChIP-Seq)

Ten-day-old *35S:S-HsfA2-GFP* transgenic *Arabidopsis* plants were treated at 45°C for 2 h following recovery at 22°C for 20 h. Two independent transgenic lines (#4 and #6) were generated and separately sequenced for each ChIP-seq. The plant samples were subjected to ChIP assays using an anti-GFP antibody (ab290, Abcam) according to the instructions for the EpiQuik Plant ChIP Kit (Epigentek). Enriched DNA was used to generate sequencing libraries using the nano-ChIP-seq protocol as previously described (Adli and Bernstein, 2001). The libraries were sequenced using the Illumina HiSeq 2500 platform at Majorbio (Shanghai, China). Following quality control of the resulting sequencing data, MACS software was used to analyse the ChIP-Seq data to obtain the peak (enrichment region) location and information. The S-HsfA2 binding motifs were identified using the MEME-ChIP tool (Machanick and Bailey, 2011). Our raw data have been deposited in the NCBI database under BioProject accession number PRJNA947075.

Protein extraction

The GST-tagged proteins (GST-S-HsfA2), GST mock proteins, His6-tagged proteins (His6-HsfA2/S-HsfA2/S-HsfA4c/S-HsfB1/S-HsfB2a/DBD/tDBD) and His6 mock proteins were purified using glutathione Sepharose 4B beads (GE Healthcare) and nickel-nitrotriacetic acid (Ni-NTA) agarose beads (CwBio, China), respectively. Total protein was extracted from plant samples according to Liu et al. (2013). Twenty-day-old *Arabidopsis* plants were left untreated (control, 22°C) or treated at 37°C or 42°C for 2 h, after which 2 g of each sample was subjected to nuclear protein extraction. Nuclear fractionation was performed based on the protocol described by Xia et al. (1997) with modifications to that of Wang et al. (2020). Protein concentrations were determined by using a SpectraMax QuickDrop and bovine serum albumin (Sigma) as the reference standards for analysis.

Western blot analysis

Proteins separated on a gel were electrophoretically transferred to a pure nitrocellulose blotting membrane (Pall Life Sciences). The membrane was cut across the molecular mass region of the corresponding proteins and separately probed with the following corresponding antibodies: an anti-β-glucuronidase (N-terminal) antibody (G5420, Sigma–Aldrich) and an anti-tubulin antibody (T5168, Sigma–Aldrich) for the expression of GUS in *HRE-35Sm:GUS*, *mHRE-35Sm:GUS*, and *35Sm:GUS* seedlings; an anti-GFP (ab290, Abcam) and an anti-mCherry antibody (ab213511, Abcam) for the detection of *35S:S-HsfA2-GFP* and *35S:HsfA2-RFP* transgenic *Arabidopsis* seedlings; an anti-GST antibody (EASYBIO) and an anti-His6 antibody (Tiangen Biotech, China) for the expression of GST- or His6-tagged proteins; an anti-histone H3 antibody (AS10710, Agrisera, Vännäs, Sweden); and an anti-UGPase antibody (AS05086, Agrisera) to verify successful nuclear protein isolation. Chemiluminescence was performed on a Fujifilm LAS-4000 imager with ECL Prime Western Blot detection reagent (Amersham Biosciences). The ImageJ analysis tool was used for grayscale analysis of the Western blot bands of GUS and tubulin.

Yeast one-hybrid (Y1H) and electrophoretic mobility shift assays (EMSAs)

Y1H and EMSA were performed as described previously (Sun et al., 2015; Wang et al., 2020).

ChIP–qPCR

Ten-day-old *35S:S-HsfA2-Flag* and *35S:HsfA2-RFP* plants were subjected to ChIP assays. The EpiQuik Plant ChIP Kit (Abcam), anti-Flag (F3165-2MG; SIGMA), anti-RFP (ab213511; Abcam) and normal mouse IgG (provided by the kit) were used for the assay. After immunoprecipitation, the enriched DNA was analysed by qPCR. Quantification was carried out using the input DNA relative to 1%. The enrichment of the ChIP target was defined as the binding rate between the immunoprecipitated

samples of the Flag and RFP antibodies and the control immunoprecipitated sample of IgG. As noted above, the binding ratio was calculated using the triangular incremental period threshold method. ChIP–qPCR for the plant materials described above was performed using the 3'-UTR as a negative control for HRE-HRE-like sequences as well as for the HSE.

DNA–protein pulldown assay

DNA pulldown experiments were performed using Pulldown Kits for Biotin-Probes (Viagene Biotech, Changzhou, China) according to the manufacturer's instructions. Briefly, equal amounts (50 μg) of GST-S-HsfA2 or His6-HsfA2 were incubated in binding buffer (50 mM Tris-HCl [pH 7.5], 100 mM NaCl, 0.1% Triton X-100 [v/v]) in a 4°C rotator for 0 h (control), 4 h, or 12 h. The corresponding samples were incubated with biotin-labelled HSE (7 ng) and 5 ng of polydeoxyinosinic-deoxycytidylic acid (dI-dC) for 40 min at 25°C. Then, the DNA/protein binding mixture was bound to streptavidin-agarose beads by incubating for 40 min at 25°C with gentle shaking and then washed three times to remove the unbound DNA/proteins. The bead-bound proteins were dissociated by boiling for 5 min in dissociation solution and analysed by immunoblotting (IB) with an anti-His6 antibody.

Yeast two-hybrid (Y2H) assay

The bait plasmid BD-S-HsfA2 and a series of AD-HSF prey plasmids were cotransformed into the Y2H Gold Cell yeast strain (Weidi, Shanghai, China). The GAL4 BD bait vector (pGBKT7) and GAL4 AD prey vector (pGAD424) combination were used as negative controls. pGBKT7-53 (BD-53) and pGADT7-T (AD-7) were transformed as positive controls. Their interaction was identified by a spot assay.

Bimolecular fluorescence complementation (BiFC) assay

Paired nYFP and cYFP constructs, *i.e.*, HsfA2-nYFP/S-HsfA2-cYFP, HsfA2ΔN-nYFP/S-HsfA2-cYFP, HsfA2ΔNΔDBD-nYFP/S-HsfA2-cYFP, GUS-nYFP (nYFP negative control)/S-HsfA2-cYFP, HsfA2-nYFP/GUS-cYFP (cYFP negative control), and GUS-nYFP/GUS-cYFP, were coinfiltrated into *N. benthamiana* leaves for 48 h. After DAPI staining for 30 min to 1 h, the YFP fluorescence signal was acquired via confocal microscopy (Axio Imager M2; Germany) under the YFP and DAPI channels.

GST pulldown assay

Equal amounts (10 μg) of bacterially expressed and purified proteins, *i.e.*, GST mock with His6 mock, GST mock with His6-HsfA2, GST-S-HsfA2 with His6 mock, or GST-S-HsfA2 with His6-HsfA2, were incubated in binding buffer (50 mM Tris-HCl [pH 7.5], 100 mM NaCl, 0.1% Triton X–100 [v/v]) overnight in a 4°C rotator (with 50 μL used as the input). Fifty microliters of GST beads were added, and the mixture was incubated at 4°C for 2 h. After washing with washing buffer (50 mM Tris-HCl, pH 7.5; 150 mM NaCl; 0.1% Triton X-100 [v/v]), the proteins were eluted with 20-30 μL of 20 mM GSH. Subsequently, with input as a positive control, anti-GST and anti-His6 antibodies were used to detect His6-HsfA2 and GST-S-HsfA2 in the pull-down samples by immunoblotting.

Dual-luciferase reporter assay

Leaves of *N. benthamiana* were infiltrated with a mixed bacterial solution of *Agrobacterium tumefaciens* (with each construct at OD_{600}=0.5) for induction using *sHSP17.6Bp:LUC* together with the paired effectors GUS-cYFP/HsfA2-nYFP, S-HsfA2-cYFP/HsfA2-nYFP, S-HsfA2-cYFP/GUS-nYFP, and GUS-cYFP/GUS-nYFP (vector control). LUC bioluminescence was detected after 48 h using D-luciferin, sodium salt (GOLDBIO) and a CCD camera (Tanon, China). LUC and REN activities were measured on an automated microplate reader (Varioskan Flash, Thermo, USA) using the Dual Luciferase Reporter Gene Assay Kit (Yeasen

Biotechnology, Shanghai, China). The LUC/REN ratio of the GUS control (GUS-cYFP/GUS-nYFP) transformed with *sHSP17.6Bp:LUC* was used as the calibrator (set as 1). Three independent experiments were performed.

Statistical analysis

Statistical Product and Service Solutions (SPSS23) and Microsoft Excel 2007 (Microsoft Corp) were used to perform one-way ANOVA, and Student's *t* tests were performed for $P < 0.05$.

Accession numbers

The *Arabidopsis* Genome Initiative numbers for the genes mentioned in this article are as follows: *HsfA2* (AT2G26150), *HsfA4c* (AT5G45710), *HSP17.6B* (AT2G29500), *YLS8* (AT5G08290), *HsfB1* (AT4G36990), *HsfB2a* (AT5G62020), and *EF-1α* (AT1G18070). The ChIP-seq data supporting the findings of this study have been deposited in the NCBI database under BioProject accession number PRJNA947075.

Acknowledgements

We thank Prof. Jing Li (Capital Normal University, China) for critical reading and valuable suggestions. This work was supported by the National Natural Science Foundation of China (grant nos. 32070546 and 31771361 to X.Q.).

Author contributions

X.Q. conceived and supervised this project. W.C., J.Z., Z.T., S.Z., X.B., and X.Q. designed the experiments and analysed the data; W.C., J.Z., Z.T., S.Z., X.B., and W.L. performed the experiments; X.Q. and W.C. prepared all figures and final datasets; and X.Q. and W.C. wrote the article with contributions from all the authors.

Data availability

All the data generated or analysed during this study are included in the manuscript and supporting files.

Supplementary data

Supplementary Figure S1. The LxLxLx motif is responsible for S-HsfA2 transcriptional repression.

Supplementary Figure S2. The constitutive expression of S-HsfA2 inhibits *Arabidopsis* seedling growth.

Supplementary Figure S3. S-HsfA2 accumulates mainly in the nucleus after heat stress.

Supplementary Figure S4. Chromatin immunoprecipitation (ChIP) combined with high-throughput sequencing revealed a motif bound by S-HsfA2-GFP.

Supplementary Figure S5. Bacterially expressed and purified GST-S-HsfA2.

Supplementary Figure S6. His6-HsfA2 fails to bind to the HRE *in vitro*.

Supplementary Figure S7. The LRD is responsible for S-HsfA4c transcriptional repression.

Supplementary Figure S8. Transactivation activity of S-HsfB1 and S-HsfB2 in yeast cells.

Supplementary Figure S9. HsfA2 binds to the HSE of the *HSP17.6B* promoter.

Supplemental Table S1. A total of 80 putative targets of S-HsfA2.

Supplemental Table S2. A list of primers used in this study.

References

Adli, M. and Bernstein, B. E. (2011). Whole-genome chromatin profiling from limited numbers of cells using nano-ChIP-seq. *Nature Protoc* **6**: 1656–1668.

Ahn, S. G., Liu, P. C. C., Klyachko, K., Morimoto, R. I., and Thiele, D. J. (2001). The loop domain of heat shock transcription factor 1 dictates DNA-binding specificity and responses to heat stress. *Genes Deve* **15**: 2134–2145.

Amin, J., Ananthan, J., and Voellmy, R. (1988). Key features of heat shock regulatory elements. *Mol Cell Biol* **8**: 3761–3769.

Baler, R., Zou, J., and Voellmy, R. (1996). Evidence for a role of Hsp70 in the regulation of the heat shock response in mammalian cells. *Cell Stress Chaperones* **1**: 33–39.

Bita, C. E. and Gerats, T. (2013). Plant tolerance to high temperature in a changing environment: scientific fundamentals and production of heat stress-tolerant crops. *Front Plant Sci* **4**: 273.

Chen, W., Shi, Y., Wang, C., and Qi, X. (2024). *AtERF13* and *AtERF6* double knockout fine-tunes growth and the transcriptome to promote cadmium tolerance in *Arabidopsis*. *Gene* **911**: 148348.

Cheng, Q., Zhou, Y., Liu, Z., Zhang, L., Song, G., Guo, Z., Wang, W., Qu, X., Zhu, Y., and Yang, D. (2015). An alternatively spliced heat shock transcription factor, OsHSFA2dI, functions in the heat stress-induced unfolded protein response in rice. *Plant Biol* **17**: 419–429.

Deng, W. G., Zhu, Y., Montero, A., and Wu, K. K. (2003). Quantitative analysis of binding of transcription factor complex to biotinylated DNA probe by a streptavidin-agarose pulldown assay. *Anal Biochem* **323**: 12–18.

Enoki, Y. and Sakurai, H. (2011). Diversity in DNA recognition by heat shock transcription factors (HSFs) from model organisms. *FEBS Lett* **585**: 1293–1298.

Feng, N., Feng, H., Wang, S., Punekar, A. S., Ladenstein, R., Wang, D. C., Zhang, Q., Ding, J., and Liu, W. (2021). Structures of heat shock factor trimers bound to DNA. *iScience* **24**: 102951.

Fragkostefanakis, S., Rth, S., Schleiff, E., and Scharf, K. (2015). Prospects of engineering thermotolerance in crops through modulation of heat stress transcription factor and heat shock protein networks. *Plant Cell Environ* **38**: 1881–1895.

Fujikake, N., Nagai, Y., Popiel, H. A., Kano, H., Yamaguchi, M., and Toda, T. (2005). Alternative splicing regulates the transcriptional activity of *Drosophila* heat shock transcription factor in response to heat/cold stress. *FEBS Lett* **579**: 3842–3848.

He, N.Y., Chen, L.S., Sun, A.Z., Zhao, Y., Yin, S.N., and Guo, F.Q. (2022). A nitric oxide burst at the shoot apex triggers a heat-responsive pathway in *Arabidopsis*. *Nat Plants* **8**: 434–450.

Hsu, S. F., Lai, H. C., and Jinn, T. L. (2010). Cytosol-localized heat shock factor-binding protein, AtHSBP, functions as a negative regulator of heat shock response by translocation to the nucleus and is required for seed development in *Arabidopsis*. *Plant Physiol* **153**: 773–784.

Hu, Y., Mesihovic, A., Jiménez-Gómez, J. M., Röth, S., Gebhardt, P., Bublak, D., Bovy，A., Scharf. K., Schleiff, E., and Fragkostefanakis, S. (2020). Natural variation in *HsfA2* pre-mRNA splicing is associated with changes in thermotolerance during tomato domestication. *New Phytol* **225**: 1297–1310.

Lin, T., Yang, W., Lu, W., Wang, Y., and Qi, X. (2017). Transcription factors PvERF15 and PvMTF-1 form a cadmium stress transcriptional pathway. *Plant Physiol* **173**: 1565–1573.

Ling, Y., Mahfouz, M. M., and Zhou, S. (2021). Pre-mRNA alternative splicing as a modulator for heat stress response in plants. *Trends Plant Sci* **26**: 1153–1170.

Littlefield, O. and Nelson, H. C. (1999). A new use for the 'wing' of the 'winged' helix-turn-helix motif in the HSF-DNA cocrystal. *Nat Struct Biol* **6**: 464–470.

Liu, J., Sun, N., Liu, M., Liu, J., Du, B., Wang, X., and Qi, X. (2013). An autoregulatory loop controlling *Arabidopsis HsfA2* expression: role of heat shock-induced alternative splicing. *Plant Physiol* **162**: 512–521.

Ma, Z., Li, M., Zhang, H., Zhao, B., Liu, Z., Duan, S., Meng, X., Li, G., and Guo, X. (2023). Alternative splicing of *TaHsfA2-7* is involved in the improvement of thermotolerance in wheat. *Int J Mol Sci* **24**: 1014.

Machanick, P. and Bailey, T. L. (2011). MEME-ChIP: motif analysis of large DNA datasets. *Bioinformatics*. **27**: 1696–1697.

Marion, J., Bach, L., Bellec, Y., Meyer, C., Gissot, L., and Faure, J. D. (2008). Systematic analysis of protein subcellular localization and interaction using high-throughput transient transformation of *Arabidopsis* seedlings. *Plant J* **56**: 169–179.

Morimoto, R. (1993). Cells in Stress: transcriptional activation of heat shock genes. *Science*. **259**: 1409–1410.

Morimoto, R. I. (1998). Regulation of the heat shock transcriptional response: cross talk between a family of heat shock factors, molecular chaperones, and negative regulators. *Genes Deve* **12**: 3788–3796.

Neueder, A., Achilli, F., Moussaoui, S., and Bates, G. P. (2014). Novel isoforms of heat shock transcription factor 1, HSF1γα and HSF1γβ, regulate chaperone protein gene transcription. *J Biol Chem* **289**: 19894–19906.

Nishizawa, A., Yabuta, Y., Yoshida, E., Maruta, T., Yoshimura, K., and Shigeoka, S. (2006). *Arabidopsis* heat shock transcription factor A2 as a key regulator in response to several types of environmental stress. *Plant J* **48**: 535–547.

Nover, N., Bharti, K., Döring, P., Mishra, S. K., and Scharf, K. D. (2001). *Arabidopsis* and the heat stress transcription factor world: how many heat stress transcription factors do we need? *Cell Stress Chaperones* **6**: 177–189.

Ogawa, D., Yamaguchi, K., and Nishiuchi, T. (2007). High-level overexpression of the *Arabidopsis* HsfA2 gene confers not only increased thermotolerance but also salt/osmotic stress tolerance and enhanced callus growth. *J Exp Bot* **58**: 3373–3338.

Satyal, S. H., Chen, D., Fox, S. G., Kramer, J. M., and Morimoto, R. I. (1998). Negative regulation of the heat shock transcriptional response by HSBP1. *Genes Deve* **12**: 1962–1974.

Scarpeci, T. E., Zanor, M. I., and Valle, E. M. (2008). Investigating the role of plant heat shock proteins during oxidative stress. *Plant Signal Behav* **3**: 856–857.

Sugio, A., Dreos, R., Aparicio, F. Maule, A.J. (2009). The cytosolic protein response as a subcomponent of the wider heat shock response in *Arabidopsis*. *Plant Cell* **21**: 642–654.

Sun, N., Liu, M., Zhang, W., Yang, W., Bei, X., Ma, H., Qiao, F., and Qi, X. (2015). Bean metal-responsive element-binding transcription factor confers cadmium resistance in tobacco. *Plant Physiol* **167**: 1136–1148.

Tanabe, M., Sasai, N., Nagata, K., Liu, X. D., Liu, P. C., Thiele, D. J., and Nakai, A. (1999). The mammalian *HSF4* gene generates both an activator and a repressor of heat shock genes by alternative splicing. *J Biol Chem* **274**: 27845–27856.

Tiwari, S. B., and Guilfoyle, H. T. J. (2004). Aux/IAA proteins contain a potent transcriptional repression domain. *Plant Cell* **16**: 533–543.

Wang, C., Gao, Z., Shi, Y., and Qi, X. (2023). Metal-responsive elements confer cadmium response in *Arabidopsis*. *Planta* **257**: 53.

Wang, C., Lin, T., Wang, M., and Qi, X. (2020). An AC-rich bean element serves as an ethylene-responsive element in *Arabidopsis*. *Plants (Basel)* **9**: 1033.

Wu, Z., Liang, J., Wang, C., Ding, L., Zhao, X., Cao, X., Xu, S., Yi, M., and Teng, N. (2019). Alternative splicing provides a mechanism to regulate LlHSFA3 function in response to heat stress in Lily. *Plant Physiol* **181**: 1651–1667.

Xia, Y., Nikolau, B. J., and Schnable, P. S. (1997). Developmental and hormonal regulation of the *Arabidopsis* CER2 gene that codes for a nucleus-localized protein required for the normal accumulation of cuticular waxes. *Plant Physiol* **115**: 925–937.

Yoshida, T., Sakuma, Y., Todaka, D., Maruyama, K., Qin, F., Mizoi, J., Kidokoro, S., Fujita, Y., Shinozaki, K., and Yamaguchi-Shinozaki, K. (2008). Functional analysis of an *Arabidopsis* heat-shock transcription factor HsfA3 in the transcriptional cascade downstream of the DREB2A stress-regulatory system. *Biochem Biophy Res Commun* **368**: 515–521.

Zhang, H., Meng, X., Li, R., Ma, Z., Liu, R., Liu, Z., Duan, S., Zhang, W., Li, G., and Guo, X. (2024). Intron retention via alternative splicing affects the thermotolerance regulation of ZmHsf17. *Physiol Plantarum* **176**: e14138.

Zhang, Y., Frejtag, W., Dai, R., and Mivechi, N. F. (2010). Heat shock factor-4 (HSF-4a) is a repressor of HSF-1 mediated transcription. *J Cell Biochem* **82**: 692–703.

Zhu, Y., Wang. Z., Jing, Y., Wang, L., Liu, X., Liu, Y., and Deng, X. (2009). Ectopic overexpression of BhHsf1, a heat shock factor from the resurrection plant *Boea hygrometrica*, leads to increased thermotolerance and retarded growth in transgenic *Arabidopsis* and tobacco. *Plant Mol Biol* **71**: 451–467.

Figures and figure legends

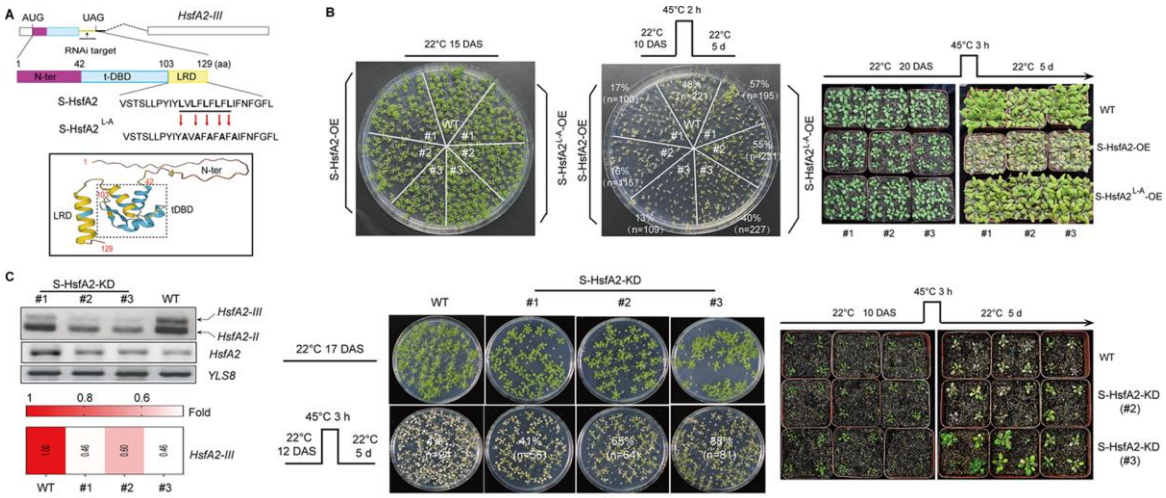

Figure 1. S-HsfA2 negatively regulates *Arabidopsis* extreme heat tolerance.

(A) Schematic diagrams of *HsfA2-III* and its corresponding product S-HsfA2 (top). Mutations in the LxLxLx motif (underlined) generated the dominant version of S-HsfA2 (S-HsfA2$^{L\text{-}A}$). The predicted AlphaFold 3D structure of S-HsfA2 (AFDB accession: AF-J7G1E7-F1) is shown (bottom). **(B)** Thermotolerance of the WT control, S-HsfA2-overexpressing (S-HsfA2-OE) lines, and S-HsfA2$^{L\text{-}A}$-overexpressing (S-HsfA2$^{L\text{-}A}$-OE) lines in both medium and soil. **(C)** RNAi-mediated S-HsfA2 knockdown (S-HsfA2-KD) and thermotolerance analyses of S-HsfA2-KD lines. RNAi (targeting the retained intron sequences; see 1A) reduced the abundance of the S-HsfA2-encoding transcript (*HsfA2-III*) but did not significantly affect the other two *HsfA2* transcripts (*HsfA2-II* and *HsfA2*) in *Arabidopsis* plants (12 DAS) exposed to 42°C for 1 h (top). YELLOW-LEAF-SPECIFIC GENE 8 (*YLS8*) served as a loading control. The RT–qPCR heatmap of *HsfA2-III* expression in three lines of S-HsfA2-KD is shown (bottom). For thermotolerance analyses, the survival rates of the seedlings under heat stress are shown. DAS, days after sowing.

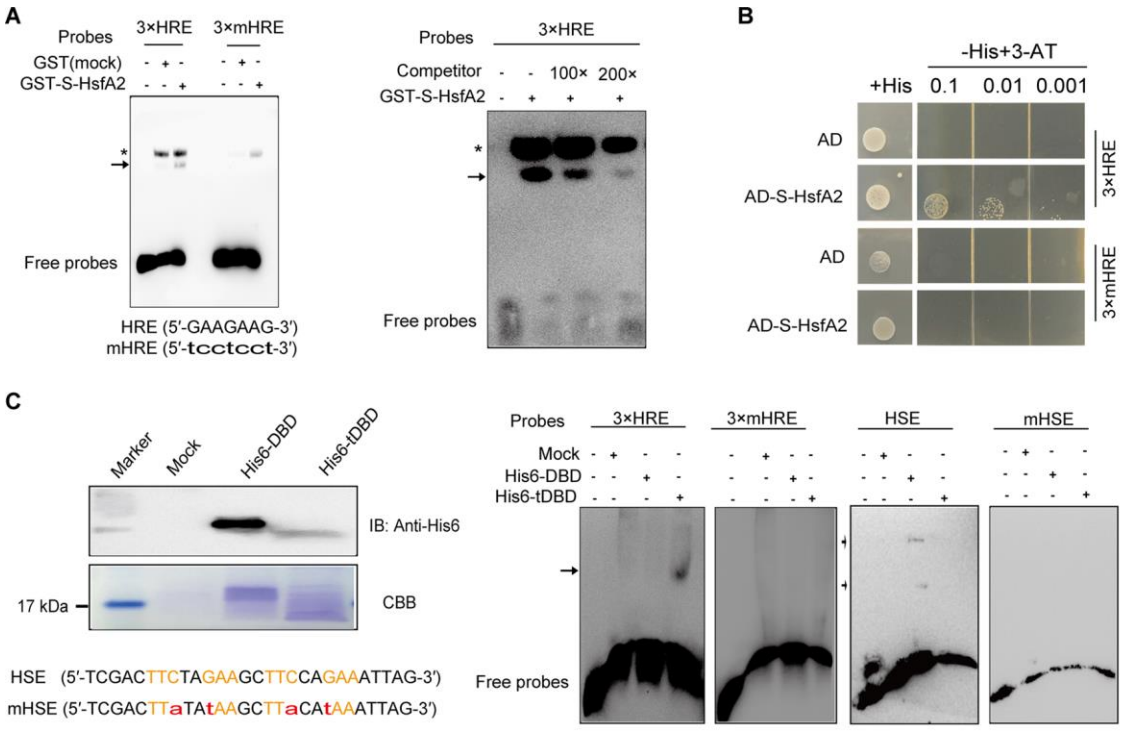

Figure 2. The HRE is recognized by S-HsfA2.

HsfA2 binding to HREs was verified by EMSA **(A)** and Y1H **(B)** assays. The mutated HRE (mHRE) was used as a negative control. **(C)** The production of His6-DBD and His6-tDBD was confirmed by immunoblotting with an anti-His6 antibody (left). The mock proteins (empty vector control) were used as a negative control. Coomassie Brilliant Blue (CBB)-stained proteins are shown as a loading control. The binding of His6-DBD and His6-tDBD to HSE or mutated HSE (mHSE) was verified by EMSA (right). For the EMSAs, the specific binding signal is marked with an arrow, while the asterisk indicates a nonspecific signal. The HRE and HSE sequences are shown, and the corresponding mutations are shown in lowercase.

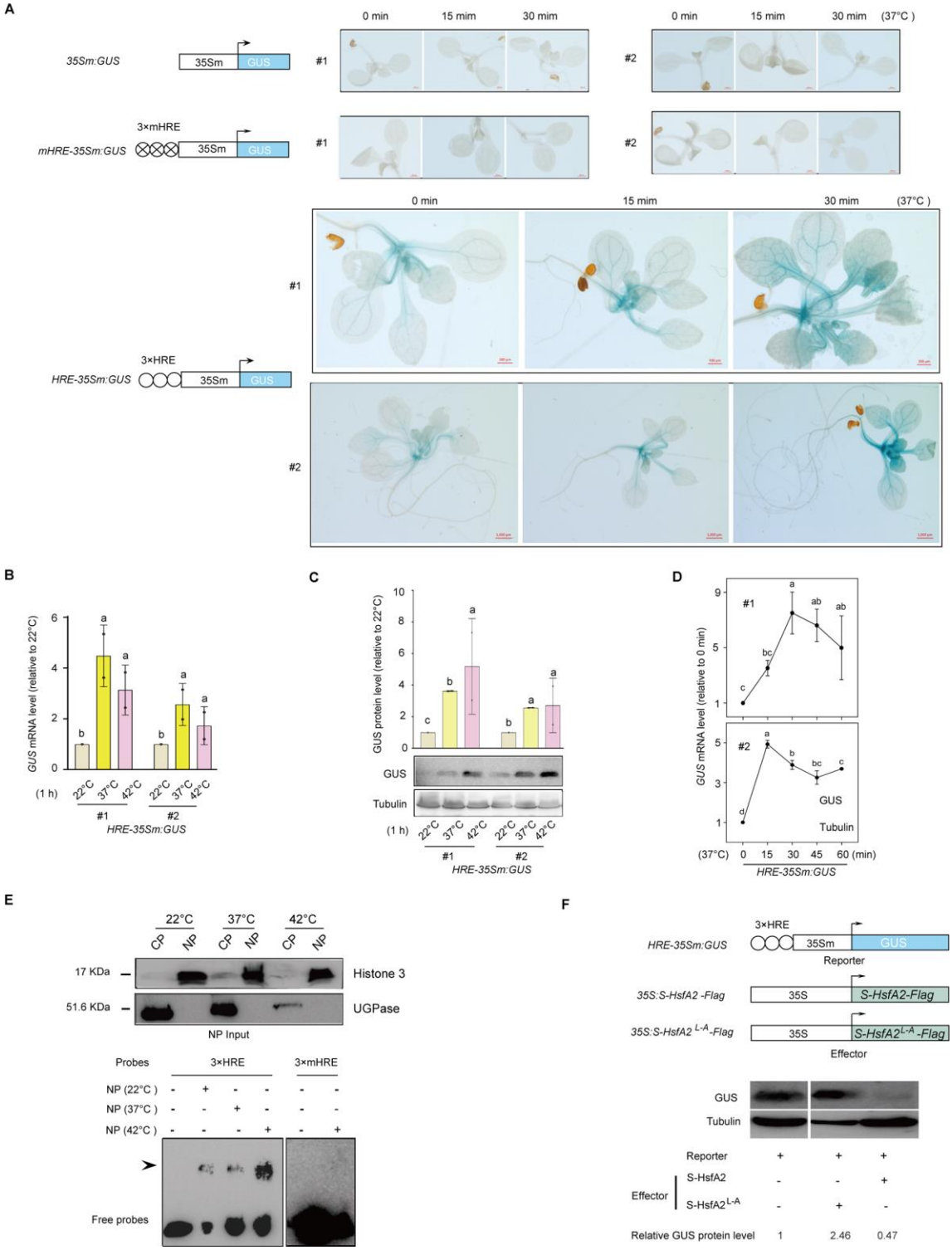

Figure 3. HRE confers heat induction in *Arabidopsis*.

(A) Qualitative GUS histochemical staining of GUS reporter transgenic *Arabidopsis* seedlings. Scale bar, 0.5 mm or 1 mm for *HRE-35Sm:GUS* (#2). Heat-induced GUS

activity analyses of *HRE-35Sm:GUS* transgenic *Arabidopsis* at the *GUS* mRNA **(B)** and GUS protein levels **(C)**. **(D)** Heat time course analysis of the *GUS* mRNA level in *HRE-35Sm:GUS* transgenic *Arabidopsis* plants. **(E)** Western blot analysis verified the successful isolation of INPUT nuclear protein (NP) without cytoplasmic protein (CP) contamination using an anti-histone H3 (nuclear marker) antibody and an anti-glucose pyrophosphorylase (UGPase) (cytoplasmic marker) antibody (top). EMSAs revealed that HRE probes, but not mHRE probes, bound to NPs from heat shock-treated (37°C, 42°C) or untreated (22°C) *Arabidopsis* plants (bottom). The bound complex is indicated by an arrow. **(F)** GUS accumulation in crossed GUS reporter plants harboring *35S:S-HsfA2-Flag* or *35S:S-HsfA2*$^{L\text{-}A}$*-Flag* effector (+effector) or an uncrossed reporter control (-effector). In **(C)** and **(F)**, GUS expression was determined by immunoblotting assays using anti-GUS and anti-Tubulin antibodies. The GUS protein level is expressed as the relative band intensity of GUS to tubulin [the control (22°C) or the effector was set as 1]. In **(B)**, **(C),** and **(D)**, the data are presented as the means ± SDs of at least two independent experiments. Different letters indicate significant differences according to one-way ANOVA, $P < 0.05$.

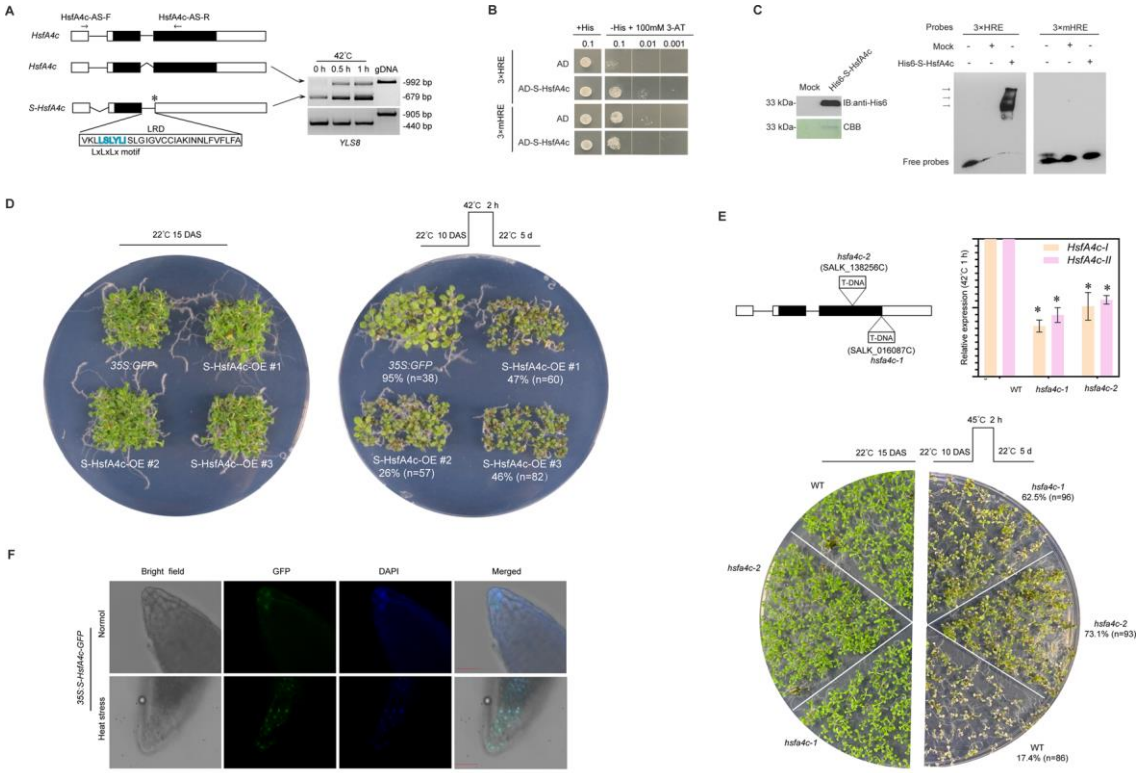

Figure 4. S-HsfA4c is similar to S-HsfA2 and represents a new HSF.

(A) Schematic diagrams of *HsfA4c* splice variants and their RT–PCR splicing analyses in two-week-old *Arabidopsis* plants under heat stress. The *YLS8* gene served as a loading control. gDNA, genomic DNA control. The asterisk indicates the in-frame stop codon. S-HsfA4c binding to the HRE was verified by Y1H **(B)** and EMSA with bacterially expressed and purified His6-S-HsfA4c **(C)**. **(D)** Thermotolerance of the *35S:GFP* vector control and *35S:S-HsfA4c-GFP* overexpression (S-HsfA4c-OE) lines. **(E)** Two T-DNA HsfA4c insert-knockdown mutants (*hsfa4c-1* and *hsfa4c-2*) confirmed by RT–qPCR (Student's *t* test, *P <0.05; top) and thermotolerance analyses (bottom). For thermotolerance analyses, the survival rates of the seedlings under heat stress are shown. **(F)** Representative images of the subcellular localization of S-HsfA4c-GFP in *Arabidopsis* root cells treated without (normal) or with heat stress

(42°C for 1 h). DAPI, 4,6-diamidino-2-phenylindole (DAPI; nuclei staining). Scale bar, 40 μm. DAS, days after sowing.

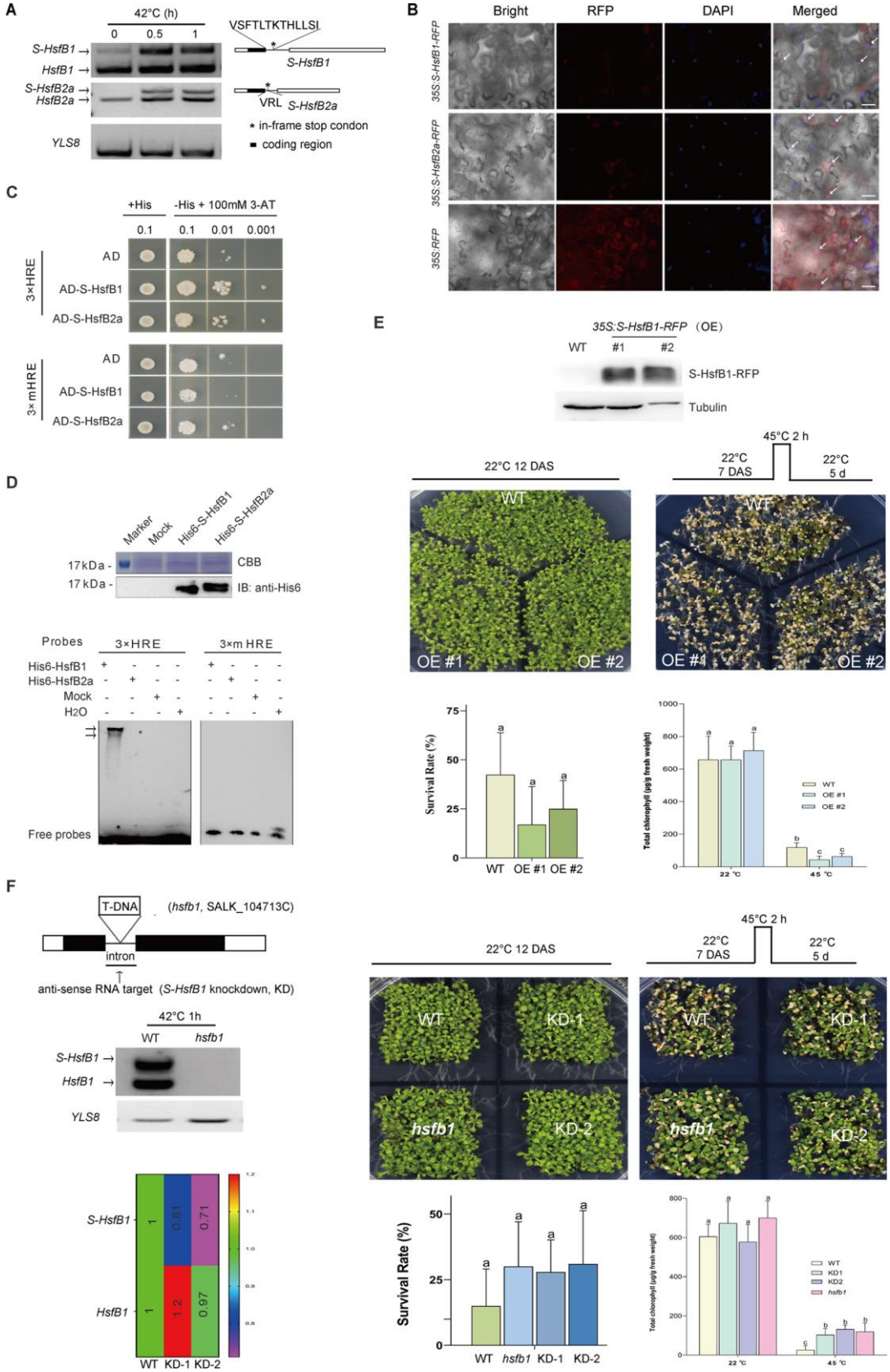

Figure 5. S-HsfB1 is similar to S-HsfA2 and represents a new HSF.

(A) RT–PCR splicing analyses of *HsfB1* and *HsfB2a* in 7-d-old *Arabidopsis* plants under heat stress. The *YLS8* gene served as a loading control. The structures of the S-HsfB1 and S-HsfB2a splice variants are shown in the right panel. The amino acid residues encoded by the retained introns are indicated above each variant. **(B)** Representative images showing the subcellular localization of S-HsfB1-RFP or S-HsfB2a-RFP in *N. benthamiana* epidermal cells. RFP was used as a negative control. DAPI, 4,6-diamidino-2-phenylindole (DAPI; nuclei staining). Scale bar, 50 μm. **(C, D)** S-HsfB1 or S-HsfB2a binding to the HRE was verified by Y1H and EMSA with bacterially expressed and purified His6-S-HsfB1 or His6-S-HsfB2a. Mock, empty vector control. **(E)** The *35S:S-HsfB1-RFP*-overexpressing (OE) lines were confirmed by western blot analysis and then subjected to thermotolerance assays. **(F)** The T-DNA *HsfB1*-knockout mutant (*hsfb1-1*) confirmed by RT–PCR and the antisense (targeting the retained intron sequences)-mediated *S-HsfB1*-knockdown lines (KD-1 and KD-2) verified by RT–qPCR were subjected to thermotolerance assays. The data are presented as the means ± SDs of three independent experiments. Different letters indicate significant differences according to one-way ANOVA, $P < 0.05$. DAS, days after sowing.

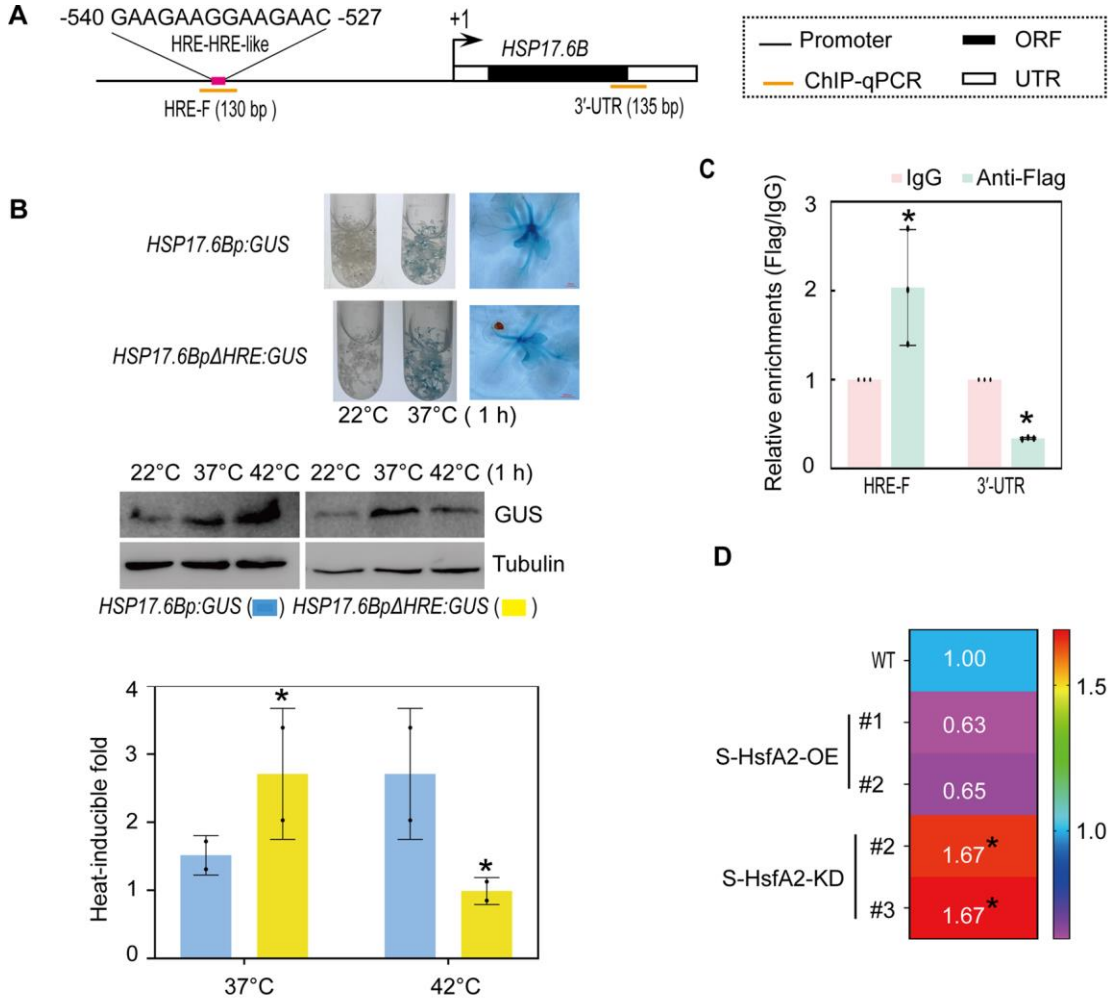

Figure 6. *HSP17.6B* was identified as a direct target gene of S-HsfA2.

(A) Schematic diagrams of the *HSP17.6B* gene (top) showing HRE-HRE-like and ChIP–qPCR products. **(B)** Heat-induced GUS expression assays of *Arabidopsis* plants harboring HSP17.6Bp or HSP17.6Bp lacking the HRE-HER-like (HSP17.6BpΔHRE)-driven *GUS* reporter transgene via GUS histochemical staining (top) and heat-induced fold (heat stress/normal) analysis, as determined via Western blotting (bottom). For each *GUS* reporter transgene, mixed *Arabidopsis* plants (10 DAS) from three independent transgenic lines were treated without (normal) or with heat stress and then subjected to GUS expression analysis. Bar, 0.5 mm. **(C)** ChIP–qPCR experiments were performed with an anti-Flag antibody and mouse IgG (mock control) in *35S:S-HsfA2-Flag* (S-HsfA2-OE) *Arabidopsis* plants. **(D)** RT–qPCR

heatmaps showing heat (45 ℃ for 3 h)-induced expression of *HSP17.6B* in S-HsfA2-OE and S-HsfA2-KD plants. In **(B)**, **(C)**, and **(D)**, the data are presented as the means ± SDs of at least two independent experiments. The significance of differences between the experimental values was assessed by Student's *t* test (*P <0.05).

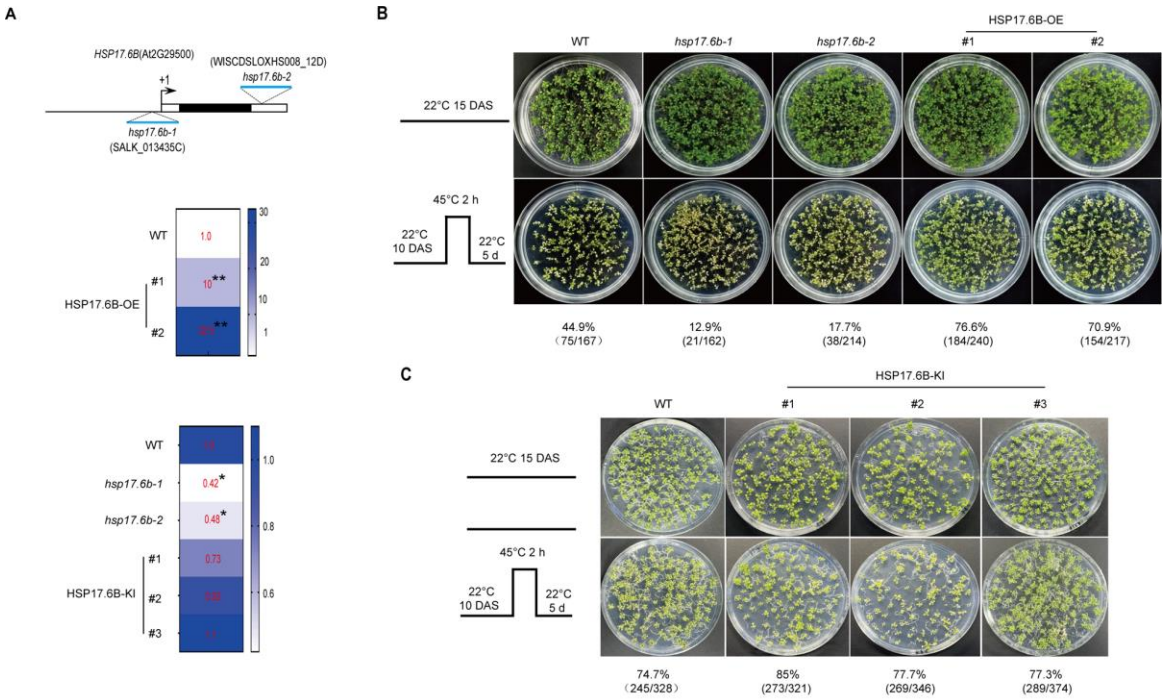

Figure 7. *HSP17.6B* positively regulates *Arabidopsis* tolerance to heat.

(A) Schematic diagrams of the *HSP17.6B* gene (top) showing T-DNA insertions. RT–qPCR heatmaps of heat (37 ℃ for 2 h)-induced expression of *HSP17.6B* in two T-DNA mutants (*hsp17.6b-1* and *-2*), three lines of *35S:HSP17.6B-Flag/hsp17.6b-1* (HSP17.6B-KI), and two lines of *35S:HSP17.6B-Flag* (HSP17.6B-OE). **(B)** Thermotolerance of the WT control, *hsp17.6b* mutants, and HSP17.6B-OE lines. **(C)** Thermotolerance of the WT control and HSP17.6B-KI lines. In **(B)** and **(C)**, the survival rates of the seedlings under heat stress are shown. DAS, days after sowing.

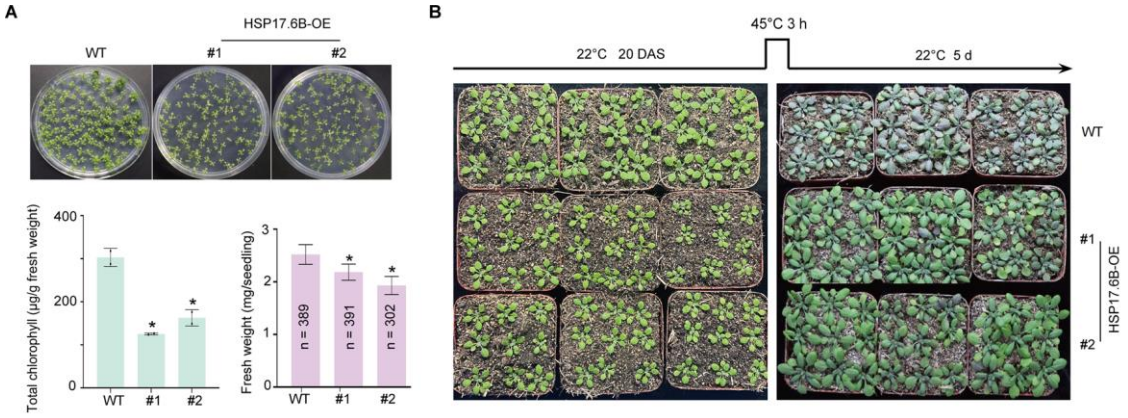

Figure 8. *HSP17.6B* overexpression represses *Arabidopsis* growth.

(A) HSP17.6B-OE plants (15 DAS) exhibited defects in growth, as indicated by decreased chlorophyll content and fresh weight. The data are presented as the means ± SDs of at least two independent experiments. The significance of differences between the experimental values was assessed by Student's t test (*P <0.05). **(B)** The dwarf but heat-resistant phenotype of the HSP17.6B-OE plants grown on soil. DAS, days after sowing.

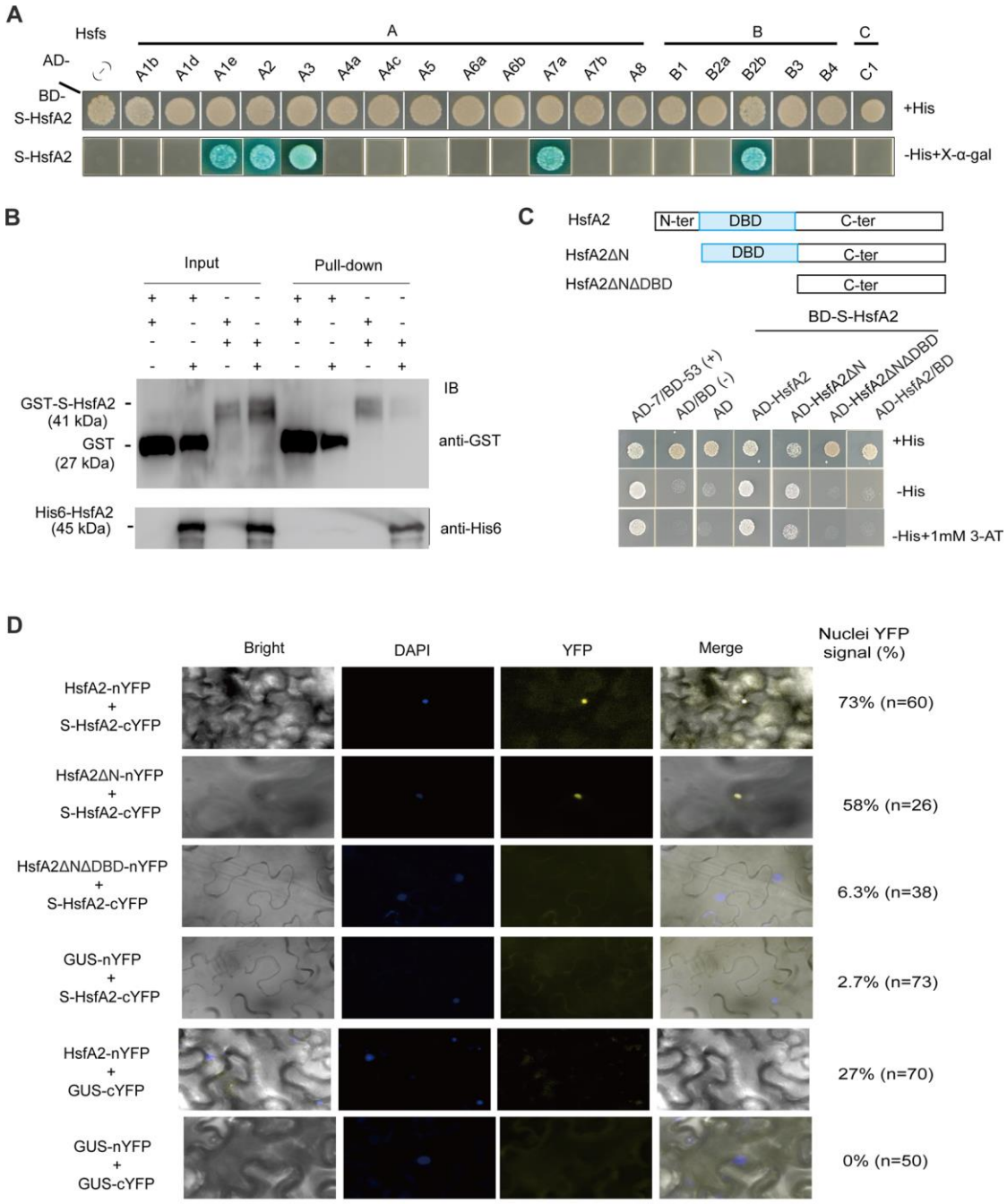

Figure 9. S-HsfA2 interacts with the DBD of HsfA2.

(A) Five HSFs that interact with S-HsfA2 were identified via Y2H analysis of 19 *Arabidopsis* HSFs. **(B)** GST pull-down verified that S-HsfA2 interacted with HsfA2 *in vitro*. According to the Y2H **(C)** and BiFC **(D)** assays, S-HsfA2 interacted with the DBD of HsfA2.

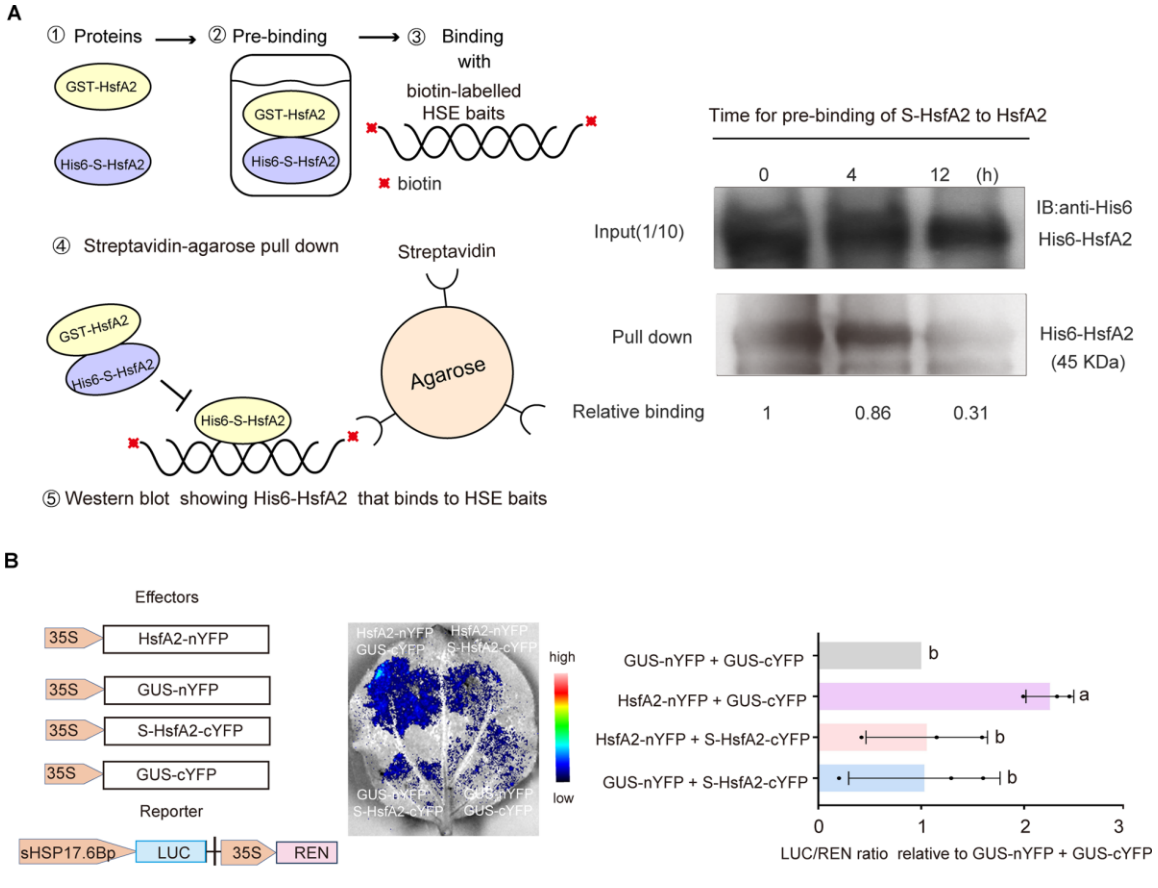

Figure 10. S-HsfA2 serves as a negative binding regulator of HsfA2.

(A) Schematic diagram of the streptavidin-agarose bead pull-down assay, in which polydeoxyinosinic-deoxycytidylic acid (dI-dC) was used as the nonspecific DNA competitor (left). GST-S-HsfA2 and His6-HsfA2 were incubated for the indicated times (0, 4, and 12 h) and then subjected to a streptavidin-agarose bead pull-down assay to isolate His6-HsfA2 proteins that bind to the biotin-labelled HSE probes. The resulting His6-HsfA2 was analysed by immunoblotting (IB) with an anti-His6 antibody (right). The ability of His6-HsfA2 to bind to the HSE bait is expressed as the relative band intensity of the control (0 h), which was set as 1. The data are the means of two independent experiments. **(B)** Dual-luciferase (LUC) assays in tobacco leaves. A representative bioluminescence image of the *sHSP17.6Bp:LUC* reporter coexpressing the indicated effector groups. The effector-driven reporter expression activity was expressed as the relative ratio of LUC to Renilla luciferase (REN) activity

(the GUS effector control was set as 1). The data are presented as the means ± SDs of three independent experiments. Different letters indicate significant differences according to one-way ANOVA, $P < 0.05$.

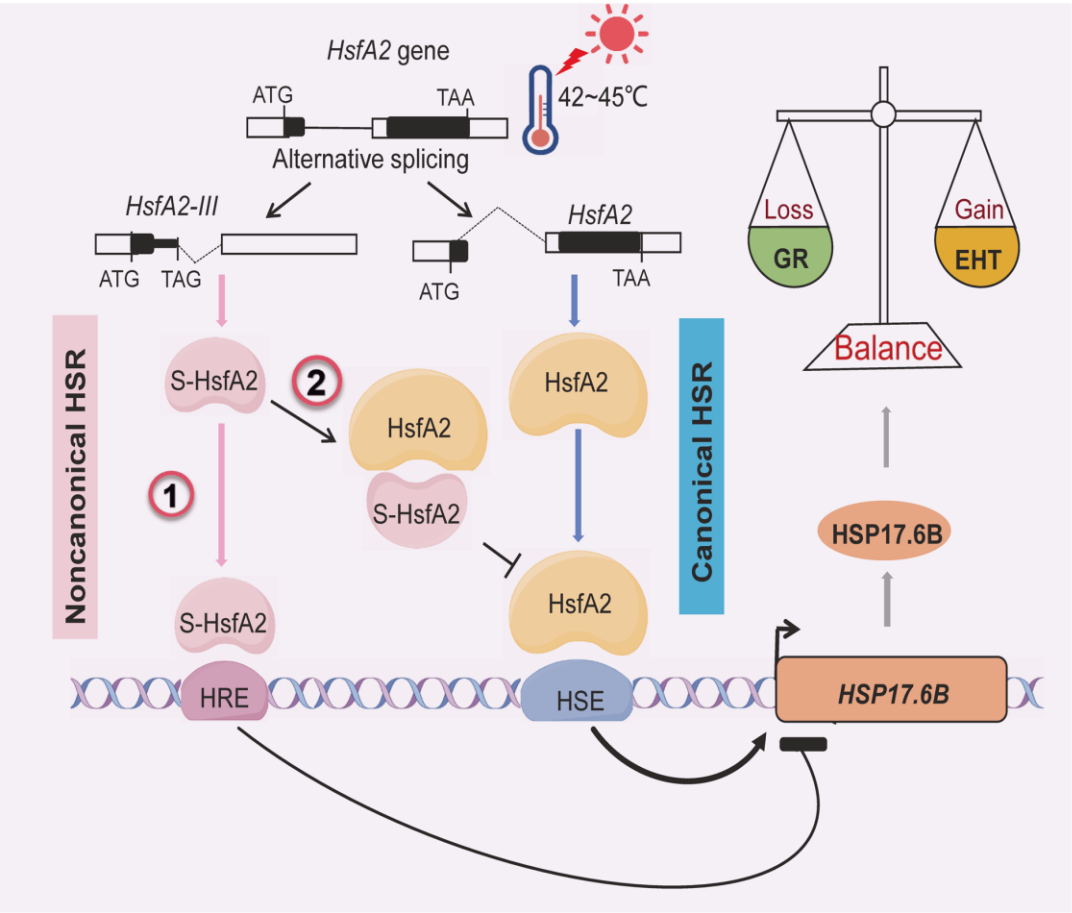

Figure 11. A proposed model for S-HsfA2 balancing *Arabidopsis* heat tolerance and growth.

The overexpression of *HSP17.6B* not only confers thermotolerance but also retards seedling growth, reflecting the hyperactivation of the HSR mediated by *HSP17.6B* overexpression. Upon exposure to severe heat, S-HsfA2 is generated from the splice variant *HsfA2-III*. Then, S-HsfA2 balances the gain (extreme heat tolerance, EHT) and loss (growth retardation, GR) of HsfA2-regulated *HSP17.6B* overexpression to ensure proper growth in two ways: ① antagonistic repression of *HSP17.6B* overexpression

through a noncanonical HSR and ② a negative binding regulator of HSFs that inactivates the *HSP17.6B* promoter-binding capacity of HsfA2.